Novel Materials for Artificial Photosynthesis

Varsha Pridhivi

Technische Universiteit Delft

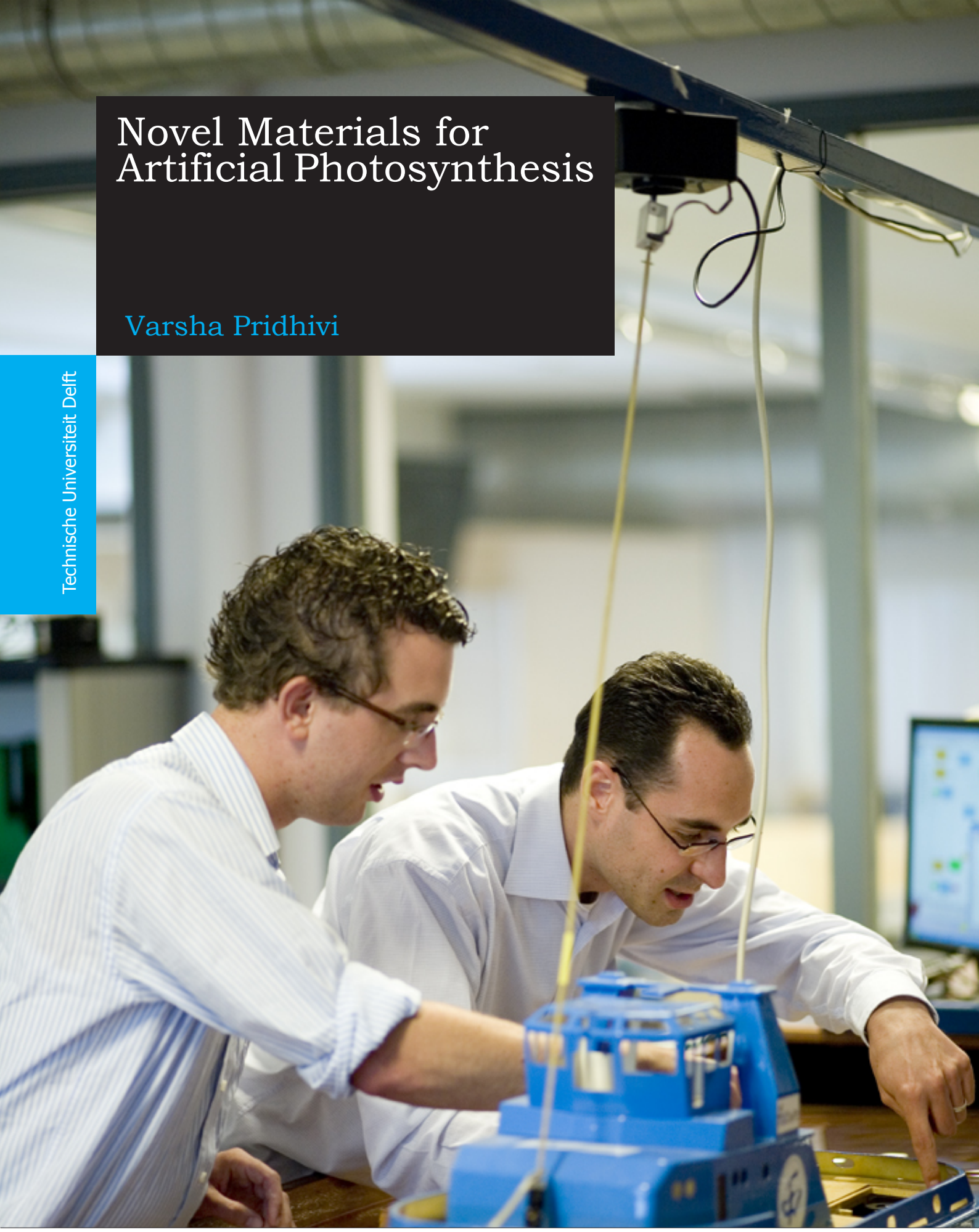

TU Delft Delft University of Technology

Challenge the future

Novel Materials for Artificial Photosynthesis

Study of light scattering mechanism of surface plasmon resonance and application in water splitting

by

Varsha Pridhivi

in partial fulfillment of the requirements for the degree of

Master of Science
in Chemical Engineering

at the Delft University of Technology,
to be defended on March 30, 2017 at 9:00 am

Student number:	4514157	
Project duration:	July 18, 2016 - March 18, 2017	
Supervisors:	Prof. dr. ir. J. Ruud van Ommen	TU Delft, PPE
	Dr. Wilson Smith	TU Delft, MECS
Thesis committee:	Prof. dr. ir. J. Ruud van Ommen	TU Delft, PPE
	Dr. Wilson Smith	TU Delft, MECS
	Prof. dr. Andreas Schmidt-Ott	TU Delft, MECS
Daily Supervisor:	Ir. Marco Valenti	TU Delft, MECS

TU Delft Delft University of Technology

Contents

Acknowledgement

I take pleasure in acknowledging the immense guidance I received from the researchers of Materials for Energy Conversion and Storage (MECS) and Process and Product Engineering (PPE) research groups of TU Delft.
I express my gratitude to Prof.Dr.Ir.Ruud van Ommen and Dr.Wilson Smith for being my supervisors for this project. Their insights in this field of research motivated me to question and evaluate my findings throughout the course of research.
I am thankful to Prof. Dr. Andreas Schmidt-Ott for accepting my invitation to be a member of the thesis evaluation committee.
This would not have been possible without the guidance of my daily supervisor, Mr.Marco Valenti who constantly encouraged me in understanding science with an open mind. His valuable advice to work with sheer passion and diligence assisted me in developing a healthy work culture in the field of research.
I am grateful to Dr. Hao Bui from PPE for performing Atomic Layer Deposition experiments in the clean room, Dr. Wiel Evers from Opto-electronic Materials (OM) research group for analysis of samples under Transmission Electron Microscope, Mr. Bartek Trzesniewski from MECS for assistance in troubleshooting spray pyrolysis equipment and Mr. Jishnu Jayaraman for assistance with the software Adobe Illustrator.
I also express my heartfelt thanks to my fellow research colleagues at MECS, Mr. Anirudh Venugopal and Ms. Manju Bhamidipati for their professional and moral support.
Finally, I would like to thank my family and friends for their continuous support and belief without which the opportunity to pursue masters degree at TU Delft would not have come true.

Varsha Pridhivi
Delft, March 2017

Abstract

To address the energy demand of the growing world population, the transition from polluting exhaustible energy sources to clean inexhaustible energy sources is imminent. Solar energy is one of the energy sources that has been studied extensively. In particular, the application of solar energy in photoelectrochemical water splitting has gained wide interest in generating hydrogen as renewable fuel.
The objective of the research is the elucidation of light scattering mechanism of surface plasmon resonance of silver. Surface plasmon resonance is the phenomenon of collective oscillation of free electrons in noble metals on electromagnetic irradiation. This property of noble metals is valorised in influencing the optical and photoelectrochemical efficiency of photoanodes of interest. In this study, n-type photoanodes, $BiVO_4$ and TiO_2 are prepared and functionalized with different sized silver nanoparticles. The influence of size of nanoparticles is investigated with respect to the ability of light scattering using UV-Vis absorption measurement and Incident Photon to Current Conversion efficiency.
The difference in optical and photoelectrochemical behaviour imparted by nanoparticle on $BiVO_4$ and TiO_2 gives insight about the light scattering mechanism and the need for spectral overlap of silver surface plasmon resonance with the bandgap of the semiconductor.

Keywords: *Surface Plasmon Resonance, Light Scattering, Photoelectrochemical Water Splitting*

1

Introduction

This document is intended to present a comprehensive work of elucidating one of the mechanisms of surface plasmon resonance of metals. This is compiled under the context of application in research about novel materials for artificial photosynthesis. It is imperative in the current generation to address the energy crisis with careful utilisation of unconventional energy resources. Solar energy is one such source of energy that has been under study and application since the past three decades. The valorisation of this energy resource is built on the fact that it is clean and inexhaustible.

1.1. Energy Challenge

With the necessity to address the increasing energy demands of the growing world population,it is essential to comprehend the energy challenge posed. To gain the momentum to facilitate the transition from a fossil fuel based economy to a green, clean energy economy, formidable research is pivotal in this regard. Echoing the demand for a sustainable future, research in the field of renewable energy has gained prime importance. The increasing consumption trend predicted for renewables over the years is to be seen as a driving force for discerning the technical and economic feasibility of the same. Figure 1.1 gives energy consumption data from the International Energy Agency based on its report in 2016 about the global picture highlighting the dependance on fossil fuels and renewables.
Concerning the factors such as energy security, sustainability, fuel emissions, fuel price and subsidies etc., the fastest growing energy sector belongs to renewables. While a plateau like trend is predicted for coal based energy consumption from figure 1.2, the increasing trend for renewables is a welcoming factor to investigate the possibilities of making it energy efficient amidst exploring range of options. The highest growth rate among the renewables over the period from 1990 to 2014 is attributed to solar energy in figure 1.3, which is optimistic considering the exploitation of an inexhaustible source of energy unlike biomass or nuclear energy source. Taking into consideration this optimistic trend related to solar energy growth, research interests in this field has been witnessing various dimensions. These include photovoltaics, solar heating, artificial photosynthesis, transport fuel technology, passive thermal technology.

1.2. Artificial Photosynthesis

Artificial photosynthesis is the process of producing hydrogen and oxygen from splitting the water molecule by the use of solar energy. This is a topic that has gained wide interest in the past four decades with increased emphasis on the path of clean energy. Sustainability

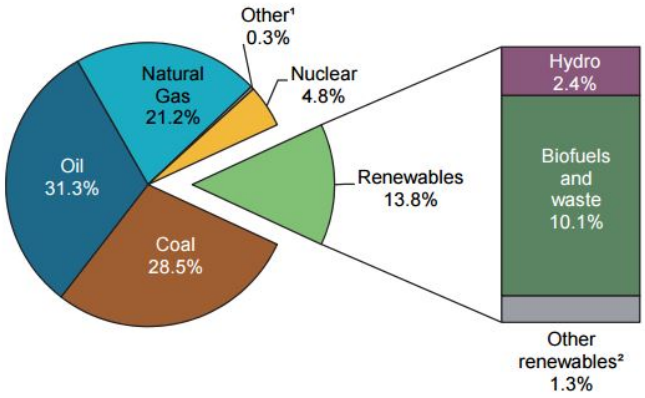

Figure 1.1: Fuel share of energy consumption in 2014. Source: International Energy Agency

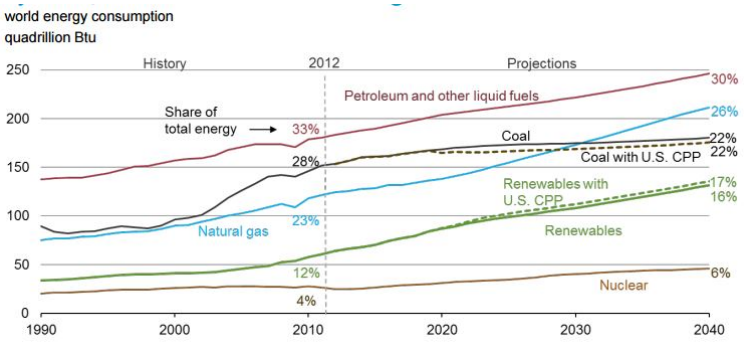

Figure 1.2: Energy consumption trend and prediction. Source: Energy Information Administration (EIS), International Energy Outlook 2016 and EIA, Analysis of the Impacts of the Clean Power Plan (May 2015)

takes predominance when addressing the ongoing energy crisis. Clearly positioning itself as an option of sustainable energy, the need for improving the technique to achieve high level of efficiency is imperative. Aiming at a society that is able to assimilate the power of a renewable source of energy to satisfy the energy demands, it is highly imminent to act and think about the nature and potential of such a source of energy. Rightly discerning the characteristics and limitations of solar energy in this perspective will offer a realistic insight to lead research. In this line of research, some of the challenges posed are related to the material of interest, efficiency, stability and socio-ecomonic barriers enroute to long term goals. Considering the material used for converting solar energy into chemical energy, the limitations that are usually associated with are low efficiency, stability, photo corrosion, low light absorption, charge carrier separation and recombination.

In photoelectrochemical water splitting, water molecule is split into H_2 and O_2 based on the conversion of solar energy to chemical energy. This technology can reduce the dependence on fossil fuels for energy needs since H_2 that is released is a potential source of clean energy. This can also be combined with the carbon capture technique where CO_2 can be used to generate syngas and other hydrocarbon fuels. The valorization of this technology is crucial for a sustainable living that caters to feasible energy demands.

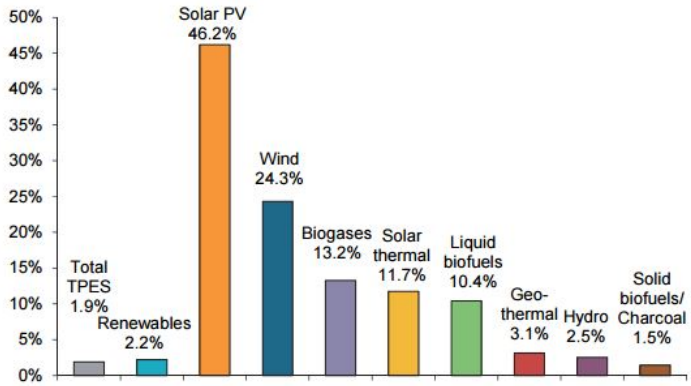

Figure 1.3: Annual growth rates of world renewables supply from 1990 to 2014. Source: International Energy Agency

1.3. Motivation

To understand the science behind light absorption using metal nanoparticles on semiconductor, research is being done in the past two decades to exploit the surface plasmon resonance of metal nanoparticles. The ability of the metal nanoparticles to exhibit different optical and electrical behaviour based on factors like size, shape, dielectric medium has effect on the surface plasmon resonance. This feature can be used when metal nanoparticles are decorated/ deosited on semiconductor surface. By establishing improved light absorption using this technique, the no. of photogenerated electron-hole pairs increase to deliver higher photocurrents through water splitting. The mechanisms by which the surface plasmon resonance work is of great concern in the field of plasmonic nanoparticles. One such mechanism which is not elucidated in detail is light scattering. An interesting feature of light scattering is the need for overlap of the semiconductor bandgap and the metal SPR to effect this. Working on a suitable semiconductor-metal combination to understand this effect forms the basis of the research.

Research questions:

- How to use light scattering mechanism in improve photoelectrochemical water splitting performance of semiconductor?
- What is the influence of size on light scattering mechanism of metal surface plasmon resonance?

By changing the size of the noble metal nanoparticle, the localized surface plasmon resonance can be tuned. Through this, the study of the effect of tuning surface plasmon resonance to obtain enhanced light absorption in semiconductors will be analysed. Hereby it is proposed to use silver nanoparticle to effect changes in the water splitting characteristics of Bismuth Vanadate ($BiVO_4$) and TiO_2. The influence of the size of nanoparticle on the optical and photoelectrochemical behaviour of the semiconductors for water splitting will be determined. In addition to this, study of effect of change in dielectric medium using TiO_2 coating on silver nanoparticles on $BiVO_4$ is also proposed.

It is proposed to use light scattering nanoparticles for analyzing the mechanism of SPR. By using nanoparticles of size which are proved to be effective in light scattering, the mechanism of SPR can be elucidated in detail.

2

Theory and literature

2.1. Photoelectrochemical Water splitting[1]

Water splitting is done by employing photochemistry on semiconductors that act as photo-catalyst. When photons of sufficient energy are incident on the semiconductor, the electrons in the valence band are excited to the conduction band. The energy needed to excite the electron should be greater than or equal to the bandgap of the semiconductor. Bandgap is defined as the difference in energy level between the valence band and the conduction band. This is found in semiconductors unlike metals where continuous energy levels are present. It ranges from the top of the filled valence band to the bottom of the vacant conduction band [5]. Subsequently, holes and electrons are formed in the valence band and conduction band respectively. These two are the charge carriers that drive the chemical reaction. Oxidation and reduction reactions occur because of the holes and the electrons respectively. Thus the solar energy is converted to chemical energy. Water splitting is carried as per the following half reactions.

At anode,

$$2\,H_2O + 4\,h^+ \longrightarrow O_2 + 4\,H^+;\, E^o = 1.23\ V\ vs\ RHE \tag{2.1}$$

At cathode,

$$4\,H^+ + 4\,e^- \longrightarrow 2\,H_2;\, E^o = 0\ V\ vs\ RHE \tag{2.2}$$

The Overall reaction is given by,

$$2\,H_2O \longrightarrow 2\,H_2 + O_2 \tag{2.3}$$

Usually, an external bias voltage is applied to drive water splitting by the semiconductor to overcome inadequate cell voltage and slow kinetics.

The photoelectrochemical cell efficiency is given as Solar-To-Hydrogen (STH) efficiency. It can be described based on energy involved or stage efficiency. Based on energy, it is given as the ratio of chemical energy derived from evolved hydrogen to the incident solar energy which is as follows

$$\eta_{STH} = \frac{\Delta G * R_{H_2}}{P * C} \tag{2.4}$$

where ΔG is the change in Gibbs free energy, R_{H_2} is the rate of hydrogen production, P is the incident power density and C is the area of illumination of the photoelectrode.

Based on stage efficiency, it is defined as the product of efficiencies involved in absorption, charge separation and catalysis stages. It is given as

$$STH = \eta_{abs} * \eta_{sep} * \eta_{cat} \tag{2.5}$$

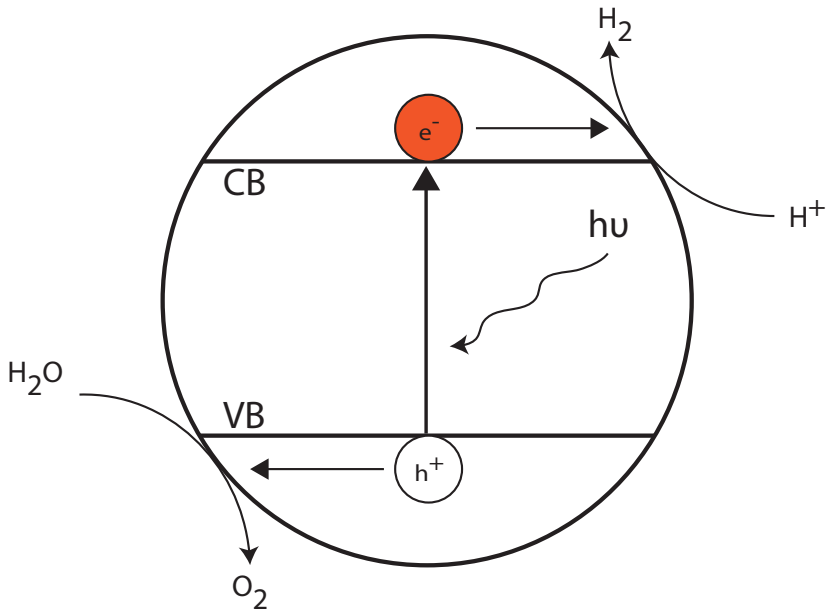

Figure 2.1: Illustration of electron hole pair involved in water splitting

where

$$\eta_{abs} = \frac{Number\ of\ photogenerated\ electron - hole\ pairs}{Number\ of\ incident\ photons} \tag{2.6}$$

$$\eta_{sep} = \frac{Number\ of\ electron - hole\ pairs\ that\ reach\ interfaces}{Number\ of\ photogenerated\ electron - hole\ pairs} \tag{2.7}$$

$$\eta_{cat} = \frac{Number\ of\ holes\ involved\ in\ water\ oxidation}{Number\ of\ holes\ that\ reach\ semiconductor\ electrolyte\ interface} \tag{2.8}$$

2.2. Semiconductor

Among a wide range of semiconductors used for water splitting, the most prominent ones are WO_3, Fe_2O_3, TiO_2, $BiVO_4$, Cu_2O, CdS, CdSe. One of the important criteria is the bandgap of the semiconductor. To attain a solar to hydrogen conversion efficiency of 10%, a semiconductor with wide bandgap of around 2.3 to 2.4 eV is needed [6]. The bandgap gives the range of photon energy that is capable for absorption and subsequent creation of charge carriers. The energy levels of the valence band and the conduction band also bear significance in that the valence band potential should be more positive than the oxidation potential of reaction and the conduction band potential should be more negative than the reduction potential of the reaction. A comparison of the band gap edges of different semiconductors against the redox potenials for water splitting is given in figure 2.2[7][8]. There are many mechanisms by which the water splitting reaction can be carried out. For example, Z scheme is the most popular method in which an oxygen evolving photocatalyst and an hydrogen evolving photocatalyst are used to facilitate the respective half reactions, with a redox mediator[9]. In this research, a single photocatalyst is used for oxygen evolution and hydrogen evolution is taken care by a transition metal. Bismuth Vanadate and Titanium oxide are used as semiconductor materials to enable water splitting in this research.

2.2.1. Bismuth Vanadate

The properties of Bismuth Vanadate are mentioned as before:

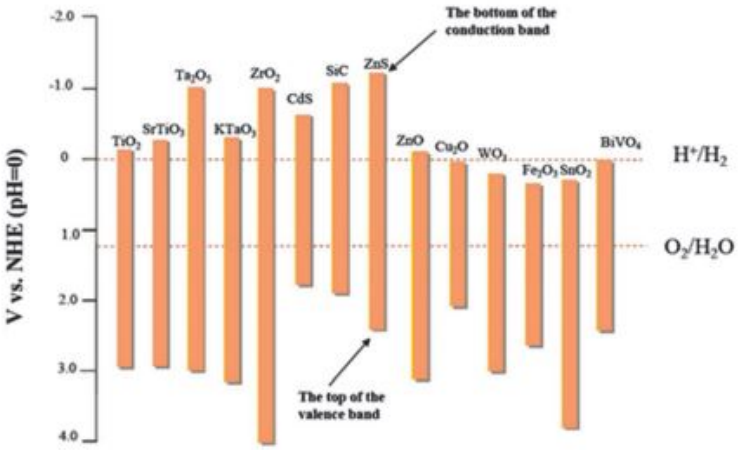

Figure 2.2: Band structure of semiconductors and redox potentials for water splitting[7][8]

- Absorption of visible light (based on favourable bandgap of ≈ 2.4 eV)[10]
- Stability in aqueous solutions[6][10]
- Position of conduction band edge below water reduction potential of 0 V vs RHE[6][10]
- Prepared from earth-abundant and non-toxic materials[10]

$BiVO_4$ is a n-type semiconductor where the photogenerated holes drive the water splitting reaction. It enjoys advantages over other semiconductors used for water splitting, such as TiO_2, CdS, CdSe, WO_3, Fe_2O_3, Cu_2O. While the bandgap of TiO_2 enables light absorption predominantly in the UV region of the solar spectrum, $BiVO_4$ absorbs light in the visible region [11]. CdS and CdSe materials as semiconductor suffer from photocorrosion and hence are unstable, while $BiVO_4$ is relatively stable in near neutral aqueous environments[11]. With a favourable conduction band edge position for water reduction, $BiVO_4$ has benefit over Fe_2O_3 and Cu_2O[12][13] .
However, there are certain limitations that are usually associated with the performance of $BiVO_4$ in water splitting. They are as follows:

- Poor charge carrier separation[6]
- Low intrinsic mobility of charge carriers[6][14]
- Slow water oxidation kinetics[3]
- Poor electron transport properties at high illumination intensity[3]

2.2.2. Advancements in improvement of performance of $BiVO_4$

Formidable efforts to address the above limitations have been made by researchers. Use of co-catalyst like Co-Pi to improve the water oxidation kinetics of $BiVO_4$ has been reported in literature[15]. To challenge poor charge carrier separation, a tungsten (W) doped gradient was employed to create a n^+-n homojunction with $BiVO_4$ as photoanode[6]. The increase in the bulk charge carrier separation was attributed to the band bending that occurs because of fermi level equilibration at the homojunction of W-$BiVO_4$ and undoped $BiVO_4$. Another interesting research dimension in photoelectrochemical cells is the design of tandem cell where different

materials are employed to perform water splitting. Configurations have involved the design of $BiVO_4$ as photoanode and Cu_2O or Si as photocathode[6][16] to improve the Solar hydrogen efficiency.

To eliminate the charge transfer caused by surface and bulk recombination, research is being conducted extensively. Employing a novel technique of prolonged exposure of $BiVO_4$ to AM1.5 simulated solar illumination in open circuit called photocharging, both surface and bulk recombination effects were subdued resulting in improvements in onset potential and photocurrent [10]. Combining different semiconductors to utilise the respective properties has also been a favoured route to achieve maximum efficieny from water splitting device. By using a heterojunction of WO_3 and $BiVO_4$ in different compositions, the solar spectrum for water oxidation was constructively used considering the light absorption in the bandgap of both the semiconductors [17]. The recombination of charge carriers generated in $BiVO_4$ was handled by the injection of the photogenerated electrons into WO_3 as the conduction band energy of $BiVO_4$ is more negative than that of WO_3. In a similar cell, doping $BiVO_4$ with Mo was also incorporated to improve the light absorption capacity of $BiVO_4$ and subsequently photocurrent density and stability. By doping Mo, the V sites in $BiVO_4$ were being occupied by Mo, changing the bandgap of semiconductor and narrowing the fermi level to enhance the generation of charge carriers under illumination and enable charge transfer to WO_3 [18]. It was also reported that among many dopants, Mo and W only were effective in increasing the photocurrent by enhancing the carrier concentration and hole diffusion length. By performing sea water splitting application, Mo doped $BiVO_4$ showed high photoresponse and photostability with RhO_2 modification in the material [19].

Apart from external modifications to the semiconductor, inherent structure modification of $BiVO_4$ was also studied in a research by creating nitrogen doping into oxygen sites by annealing. Facilitating a reduction in the bandgap energy by 0.2 eV and elevation in valence band maximum, the charge carrier density and transfer were increased[20]. In yet another fashion to modify the structure of $BiVO_4$ to enhance charge carrier separation, nanoporous structure with high surface area was prepared with particles smaller than the hole diffusion length. To further improve the photocurrent density and decrease the onset potential, oxygen evolution catalysts FeOOH/ NiOOH were deposited on $BiVO_4$, and an additional surface recombination at the $BiVO_4$/oxygen evolution catalyst interface was noted to influence the photocurrent density alongside slow water oxidation kinetics [21].

2.2.3. Titanium dioxide

Titanium oxide is one of the widely studied semiconductor materials for photocatalytic water splitting and photodecomposition of organic matter. It was the first reported semiconductor to exhibit photocatalytic activity[22]. Applications have found relevance in dye sensitized solar cells as an alternative to photovoltaic devices in terms of ease of fabrication and cost[23][24][25] where a metal dopant transfers electrons to the conduction band of the semiconductor and is recharged by electron donors in the solution.The properties of TiO_2 are as follows

- Wide bandgap of $\approx$ 3.2 eV allowing absorption in the UV-region ($\approx$ 4% of solar spectrum) [26]
- Excellent chemical stability and reactivity[26]
- Effect of cyrstallinity on photoelectrochemistry[27]

2.2.4. Advancements in improvement of performance of TiO_2

Efforts to facilitate water splitting using TiO_2 have resulted in interesting combinations of material modifications. Using RuO_2 as a photocatalyst to enable oxygen evolution and Pt for hydrogen evolution on TiO_2 surface have been demonstrated[28]. With a major drawback of a wide bandgap, the potential to use the visible region of the solar spectrum is greatly reduced. The practical application of the semiconductor to impart green energy transition also takes a backseat due to this.

To improve the light absorption to the visible region, doping of TiO_2 with Fe, Ru, Mo, V, Rh, C, S, F have been studied[29]. Doping with metal ions have been known to modify photoactivity, recombination rates and interfacial electron transfer rates[29]. N-doped TiO_2 study also revealed that bandgap narrowing of TiO_2 was possible impacting the visible light absorption, by altering the band structure[26]. Doping with strontium ions resulted in the shifting of the conduction band of TiO_2 relatively negative, thus enhancing electron hole separation and reducing recombination in the dye sensitized solar cell[30]. Doping with transition metals such as Cr and Co have resulted in bringing modification in the behaviour of opto-electronic property of TiO_2 by inducing charge carrier transport form the metal to the semiconductor conduction band[31][32].Study of Al-doping and Cr-doping of TiO_2 suggested that improved carrier diffusion length in the semiconductor attributed to high quantum efficiency and visible light absorption respectively. The formation of impurity band below the conduction band of TiO_2, changing the band structure was reported[32]. Although the utility of visible light region was reported, the decrease in photoreactivity and charge carrier efficiency with Al, Cr and Co doping was also observed raising questions about the effect of dopant. The behaviour of dopants was noticed as roles mediated between interfacial trap sites and recombination centres at low and high light intensities respectively alongside other factors such as dopant concentration, d electron configuration and distribution within the semiconductor lattice[29][26].

Structural changes for applications in photocatalysis to overcome short minority carrier diffusion length in TiO_2, study was performed on synthesis of mesoporous nanocrystalline TiO_2 films with pore size distribution in the range of carrier diffusion length[33] prior to study of influence of plasmonic nanoparticles on photocatalytic water splitting[34].

Apart from doping, the use of mixed metal oxides by anodizing metals to form composite materials has also been investigated. Nanotube arrays made of Ti-Nb-Sr-O mixed oxide delivered higher photocurrents than bare $TiO_2$by reducing recombination losses[35].

2.3. Localized Surface Plasmon Resonance[2]

To improve the efficiency of the material in absorbing light, various modifications are prevalent. One such treatment is the application of metals in the semiconductor substrate. The use of metals in this way has garnered wide interest to understand and enhance the optical and electrical properties of the semiconductor. Metals are generally incorporated to enhance the catalytic or bulk properties of semiconductor. These are addressed by the use of metal nanoparticles. By using metal in the nanoparticle form where the physical, chemical, optical and electrical properties vary as compared to bulk metal, there exists the option of tunability to serve better functionality in metal-semiconductor material. Decorating metal nanoparticles on the semiconductor/ electrolyte interface is of interest here.

Surface plasmon resonance is a feature in metals which is defined as collective oscillations that occur in the conduction band of the metals on electromagnetic irradiation. When the incident light of particular frequency strikes the interface between materials of positive and negative dielectric values, the electrons on the surface start oscillating based on the natural frequency matching the resonant frequency. These oscillations influence the electric field of the surrounding environment and are important in inducing energy transfer/ charge transfer.

A schematic illustration of surface plasmon resonance is given in figure 2.3 The absorption of the photons to facilitate this phenomenon is seen as a loss in intensity of the reflected light. Localized surface plasmon resonance, as it is referred to, creates this oscillating electron field with a lifetime of femtoseconds to result in radiative or non radiative decay. To avoid confusion about the bulk plasmon excitations that occur in the metal, it is also referred as particle surface plasmon resonance.

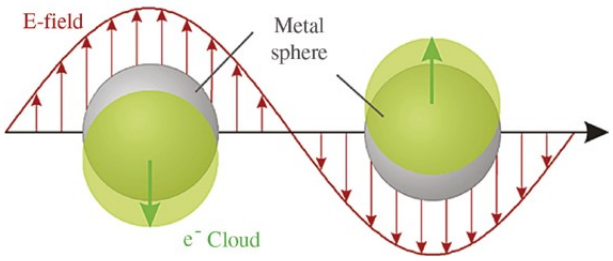

Figure 2.3: Schematic illustration of Surface Plasmon Resonance[36]

2.4. Absorption and Scattering Cross sections

It is imperative to understand the theory behind light scattering before going for the application based on the same. Well known theory on the electromagnetic interaction of metals is given in the form of Mie theory. It corresponds to the solutions to the Maxwell's equation and is widely regarded as benchmark literature available as a simple solution. Analytical expressions have been obtained as a result for absorption and scattering cross sections for spherical nanoparticles, the solution is approximated as follows[37],

$$\sigma_{abs} = k\,Im\,(\alpha) \tag{2.9}$$

$$\sigma_{sca} = \frac{k^4}{6\pi}\,|\alpha|^2 \tag{2.10}$$

where α is the particle polarizibility

$$\alpha = 3V_p \frac{\epsilon - \epsilon_M}{\epsilon + 2\epsilon_M} \tag{2.11}$$

This approximation is valid for spherical particles limited between $ak \ll 1$ and $m|ak \ll 1$ where ϵ and ϵ_m are the dielectric constants of the nanoparticle and the surrounding medium respectively. In case of a shape that is non-spherical such as ellipsoid or rod, a geometric factor is also included in the particle polarizibility expression. It is given as L_i in the following equation where it can take values along direction i like 1,2,3 summing to 1.

$$\alpha_i = V_p \frac{\epsilon - \epsilon_M}{\epsilon + L_i(\epsilon - \epsilon_M)} \tag{2.12}$$

For a spherical particle, L_i is $\frac{1}{3}$
From the above equations, factors affecting the absorption and scattering cross section and inturn surface plasmon resonance of the metal nanoparticles can be identified as the size, shape and dielectric constant. By altering these variables, tuning of surface plasmon resonance of metal nanoparticles for different applications have derived immense research outcome[2].

One of the simple variations to do is change in volume of the particle. While the absorption cross section is proportional to V_p, the scattering cross section is proportional to $V^2{}_p$. Usually the extinction cross section which is the sum of the absorption and the scattering cross section is represented for understanding. The frequency at which the nanoparticle extinction spectrum is highest is termed as the plasma resonance frequency. With change in the properties affecting the cross section, either a red shift or blue shift in the spectrum is noticed. Figure 2.4 gives a better understanding of how the size, shape and material affect the extinction spectrum.

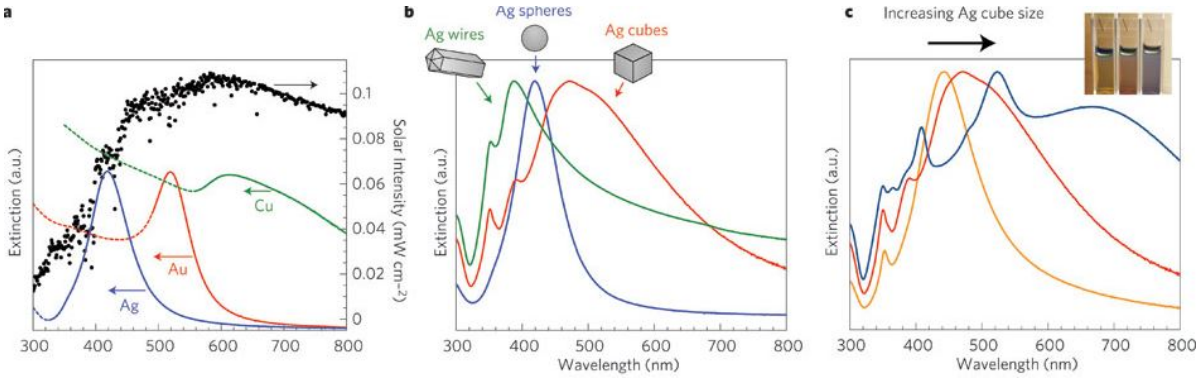

Figure 2.4: a)Normalized extinction spectra of spherical Ag (38 ±12 nm diameter), Au (25 ±5 nm) and Cu (133 ±23 nm) particles. The intensity of solar radiation (data for air mass 1.5 solar spectrum from the National Renewable Energy Laboratory, http://rredc.nrel.gov/solar/spectra/am1.5/) is also shown, in black. Dashed portions of the metal extinction curves indicate interband transitions (that is, no surface plasmon resonance in these regions). b) Normalized extinction spectra for Ag wire, cube and sphere nanoparticles. Wire-shaped particles are 90 ±12 nm diameter and >30 aspect ratio, cubic particles are 79 ±12 nm edge length and spherical particles are 38 ±12 nm diameter. c) Normalized extinction spectra for Ag nanocubes as a function of size (56 ±8 nm, 79 ±13 nm and 129 ±7 nm edge lengths correspond to orange, red and blue spectra respectively). The inset shows a photograph of the three nanocube samples suspended in ethanol[34].

From figure 2.4, it is seen that different metals exhibit plasmon resonance in different wavelength ranges according to their shape. With increase in size, the plasmon resonance wavelength red shifts, which is an important aspect for this research.

2.5. Mechanism of SPR decay

Radiative decay gives rise to photons whereas non radiative effect gives electron-hole pairs due to interband or intra band transition. The four different mechanisms by which surface plasmon resonance works are

- Light concentration
- Light scattering
- Hot Electron Injection
- Plasmon induced resonant energy transfer

Light concentration is a radiative decay mechanism by which the incoming photons create SPR in the metal nanoparticle and in turn induce the enhanced electromagnetic field to generate electron hole pairs in the semiconductor. The role of nanoparticles is to act as optical antennas in enhancing light concentration[38]. In light scattering mechanism, the photons are scattered

by the nanoparticle into the region of higher refractive index, here the semiconductor whose refractive index is higher than that of air. This results in increase in the optical path length inside the semiconductor, thereby enhancing the generation of electron hole pairs[39]. Light scattering and light concentration mechanisms are collectively called as light trapping mechanisms as they focus the incident photons on inducing/ enhancing light absorption. In non radiative SPR decay by hot electron injection, the metal nanoparticles absorb the incoming photons and inject the generated electrons into the semiconductor conduction band and the separation of the hot electrons from holes aids in water splitting [40].Introducing the plasmonic properties of noble metals such as Ag and Au on TiO_2, the efficiency of driving water splitting reactions was increased by injection of hot electrons from the metal to the semiconductor [41][42]. In the case of Plasmon Induced Resonant Energy Transfer (PIRET) mechanism, there is dipole-dipole coupling between the SPR of metal nanoparticle and transient exciton of the semiconductor[43][44].

Studying the light scattering mechanism of SPR is the objective of the research. To understand this from application point of view, the concept of front illumination and back illumination are presented as in figure 2.5 In front illumination, the coated nanoparticles are exposed to

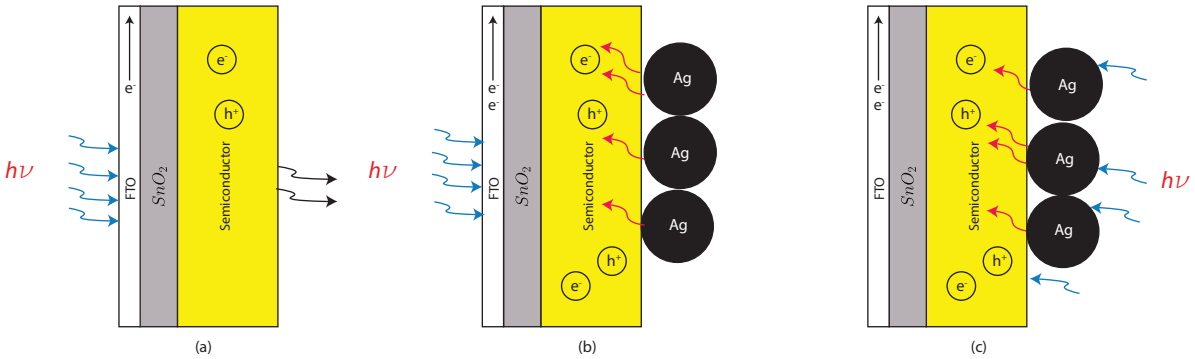

Figure 2.5: Schematic illustration of photoanode a)bare $BiVO_4$ b)$BiVO_4$ with nanoparticles for back illumination c)$BiVO_4$ with nanoparticles for front illumination. Blue arrows indicate incident photons, red arrows indicate scattered photons, blacks arrow indicate transmitted photons

light, the light that is unabsorbed by the nanoparticles reach the semiconductor substrate which inturn absorbs the light according to its bandgap. In back illumination, the light first reaches the semiconductor first and the light that is transmitted after the layer is available for absorption by the coated nanoparticles.

2.5.1. Advancements in understanding Surface Plasmon Resonance

The size influence of silver nanoparticle on $BiVO_4$ light absorption was studied to understand the mechanisms of hot electron injection and light scattering. It was reported that for smaller (less than 20 nm) metal plasmonic nanoparticles, the near field effects dominated. It was seen that the scattering cross-section of $Ag@SiO_2$ (Ag core and SiO_2 shell) was greater than its absorption cross section. To minimize the near field effect, it was essential to optimize the metal-semiconductor interfacial area. The near-field effect was based on the light concentration and plasmon induced resonance energy transfer mechanism [45].In another instance, with the deposition of light scattering Ag nanoparticles on $BiVO_4$ semiconductor substrate, it was reported that for front illumination, there was no screening by the nanoparticles to the semiconductor. It was inferred that the screening of light to the semiconductor by smaller sized light absorbing nanoparticles could be inhibited by the usage of higher sized nanoparticles[39]. Hence for semiconductor such as $BiVO_4$ which is limited by light absorption, larger sized metal

nanoparticles should be used to focus on light scattering.

In instances where surface plasmon resonance of noble metals was employed in improving the performance of semiconductor TiO_2, gold has been extensively studied. By using gold nanoparticles as plasmonic materials on N,F-doped TiO_2, the photocurrent was increased in the visible region owing to near-field effect of surface plasmon resonance of the metal[46]. The combination of defect states introduced by doping and gold SPR was exploited to improve visible light absorption. The mechanism behind the SPR of gold was plasmon induced resonant energy transfer which induced electromagnetic enhancement within the short minority carrier diffusion length. However, decrease in photocurrent in the UV region by TiO_2 functionalized with gold was because of reduced photon flux and less surface area contact with the electrolyte. Application of this mechanism was also reported in the analysis of water splitting on N-doped TiO_2 with silver nanocubes/ gold nanospheres[47]. Silver nanocubes with higher extinction efficiency than gold nanospheres based on extinction cross section and geometric cross section enabled TiO_2 in generating higher photocurrents in the visible light region. The ability of N-doped TiO_2 to perform optically stronger in the region of silver SPR than in that of gold implies the application in selecting spectral overlapping materials for improved performance. In addition to plasmon induced resonant energy transfer mechanism, radiative light scattering by silver nanocubes was reported to induce high electric field at TiO_2 surface enabling increase in optical path length.

Research on studying the scattering efficiency of metals such as silver, gold and copper have resulted in understanding the red shift with alloying and change in the surrounding refractive index. The broadness of the SPR spectrum was attributed to the alloy which found application in tuning the SPR of the comprising metals. Core-shell structure of the formed alloy found its influence in tuning the SPR and altering the intensity [48]. The influence of shape on light scattering metal plasmonic nanoparticles was analysed where cylindrical and hemispherical particles showed better optical path length enhancements than spherical particles[49]. In a study to understand the effect of dielectric medium, change in refractive index of the surrounding was employed. The change in the refractive index of the surrounding caused a red shift in the SPR of silver. The change was brought by solvent layer covering the silver nanoparticles. A linear relationship between the LSPR max wavelength and the refractive index was obtained, though there was no convincing explanation to the discrepancy to the difference in the theoretical and experimental results. The effect of oxide layer was touted to be the reason behind the discrepancy [50]. The magnitude of the red shift caused by changing the refractive index of the surrounding medium is dependent of shape, size and the mode of excitation. It was proven that triangular shaped nanoparticles were more sensitive to shift in SPR peak due to change in refractive index when compared to spherical nanoparticles [51].The effect of substrate in altering the dielectric properties was studied on the SPR of silver. Substrates with different refractive indices were used to change the dielectric properties of silver, which was seen as a change in the extinction spectrum of silver nanoparticles. The red shift in extinction spectra with increase in refractive index was verified yet again. The discrepancy in the difference in the experimental and theoretical calculations was because of the effect of true shape of the nanoparticle and the chemical nature of nanoparticle with the exposed solvent. The sensitivity with respect to the change in the solvent was more than that brought by the change in the substrate because of the area of exposure of the silver nanoparticles to the solvent being larger than that to the substrate[52].

The effect of the medium surrounding the silver nanoparticle in altering the SPR peak wavelength being more than that by the substrate itself was verified in another instance[53]. In coating TiO_2 on silver, red shift was noticed in the SPR wavelength of silver. With a thin

coating, there was not just a red shift in the SPR wavelength, but also an increase in absorption. This increase in absorption was attributed to TiO_2 which has a bandgap of 3.2 eV[54]. In the presence of coating, a linear increase was noted in the SPR wavelength against the silver layer thickness. The tunability of silver SPR was valorized by changing silver layer thickness, which was marginally less than that obtained with coating. Thus coating helped in an order of magnitude increase in SPR wavelength tunability range. To understand the influence of coating thickness, TiO_2 coating of increasing thickness on silver nanoparticles was studied. It was inferred that coating beyond a particular distance called the sensing distance would result in no shift in silver SPR wavelength, as the coating is far from the SPR field at the silver surface[55][56].

2.6. RHE potential

Applied bias potential in photoelectrochemical experiments are represented against the reversible hydrogen electrode. 0V vs RHE is referred to the hydrogen evolution potential i.e, reduction of H^+ ions to H_2. Since the effect of pH is taken into consideration in the calculation, it is more convenient than the usage of NHE potential. Denoted as E_{RHE}, it is given as[1]

$$E_{RHE} = 0.059 * pH + E_{Ag/AgCl} + E_{CE} \tag{2.13}$$

where E_{RHE} = 0.197 V vs NHE

2.7. Quantum Efficiency

External Quantum Efficiency

External Quantum Efficiency is denoted by the term IPCE which stands for Incident Photon to Current Efficiency. It is used to quantify the efficiency of current conversion obtained from the photons incident on the sample. The difference between IPCE% from 100% determining the loss, is the sum of the incident photons that are reflected or transmitted and the number of recombined photogenerated electron–hole pairs, thus unavailable for water splitting.
IPCE% is calculated as follows[1]

$$IPCE(\lambda)\% = \frac{hc}{e} \frac{j_{photo}\lambda}{\lambda P(\lambda)} * 100 \tag{2.14}$$

Internal Quantum Efficiency

Internal Quantum Efficiency is denoted by the term APCE which stands for Absorbed Photon to Current Efficiency. It quantifies the efficiency of current conversion obtained from the photons absorbed by the sample. It is ideal to validate optical performance with photoelectrochemical performance. The difference between APCE% and 100% is attributed only to recombination of charge carriers, since it is corrected for reflection and transmission losses.
APCE% is calculated as follows [1]

$$APCE(\lambda)\% = \frac{IPCE(\lambda)}{A(\lambda)} \tag{2.15}$$

3

Materials and Methods

The experimental setup to study light scattering mechanism of surface plasmon resonance was based on the following:

- Preparation of Bismuth Vanadate
- Synthesis of silver nanoparticles
- Preparation of Titanium dioxide
- Absorption via UV-Vis spectroscopy
- Photoelectrochemical cell

It is to be noted that the demineralized water (18.2 $M\Omega$ @ 25^{o}C, Q-Pod, Milli-Q) was used in the preparation of precursor solutions/ electrolyte.

3.1. Preparation of Bismuth Vanadate[3]

Bismuth Vanadate was prepared by following a well defined procedure of spray pyrolysis. Fluorine doped tin oxide(FTO)(TEC-15, Hartford Glass Co.) glass was used as substrate. A 5cmx5cm FTO glass was cleaned with a solution of soap, ethanol and sulfuric acid before ozone cleaning for a period of 45 minutes. 200 ml precursor solution was prepared from a 4mM solution of $Bi(NO_3)_3.5H_2O$(98%, Alfa Aesar) in acetic acid(98%, Sigma Aldrich) and $VO(AcAc)_2$(99%, Alfa Aesar) in absolute ethanol(Sigma Aldrich). Initially, SnO_2 layer of approximately 80 nm was deposited on FTO glass at 375 ^{o}C. This is to prevent recombination centers at the FTO-$BiVO_4$ interface. On top of the SnO_2 layer, the precursor solution was sprayed to produce a layer of 200 nm with a spray rate of 5s per cycle of 60s. The samples were annealed for 2h at 450^{o}C in air to get cystralline form of $BiVO_4$, which is important for it to exhibit photoactivity. A schematic illustration of spray pyrolysis setup is given in figure 3.1

3.2. Synthesis of silver nanoparticles

Silver nanoparticles were synthesized by a gas phase process. Gas phase synthesis of nanoparticle has several advantages over liquid phase synthesis process. Some of them include purity, continuous mode of synthesis, no need of hazardous liquid precursors and removal of residue[58][59][60][61]. In this study, silver nanoparticles were generated by the method of spark discharge. Process flow diagram in figure 3.2 gives an insight to the generation, flow, selection and deposition of nanoparticles. Generation of nanoparticles was facilitated

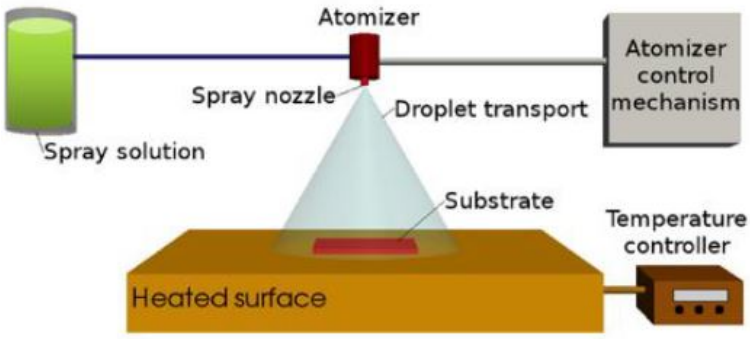

Figure 3.1: Schematic Illustration of spray pyrolysis setup[57]

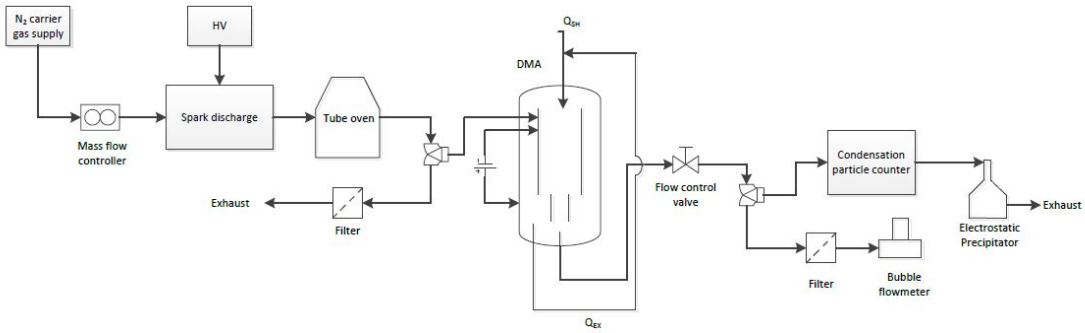

Figure 3.2: Process flowsheet for synthesis of silver nanoparticles by spark discharge

by a high voltage spark in between silver electrodes(Silver rod, 99.997%, 6 mm in diameter, Goodfellow) that are housed in the spark chamber. Spark discharge process has proved to be a simple, easy and effective process technique to give a narrow size distrubution of generated nanoparticles.The circuit in usage was a resistance-capacitance-inductance circuit. The capacitor was charged by a high voltage generator and once the breakdown voltage was attained, a spark was induced between the electrodes. The electrodes which were separated by a gap of $\approx$ 1mm, ablated under the spark to produce vapours of silver. The gap distance was maintained by altering the micrometric screw on the ground electrode. These vapours were cooled by nitrogen gas flow at room temperature in the spark chamber to condense them to form nanoparticles of different sizes. These nanoparticles that were formed, have gone through the phase of growth from primary particles to agglomerates. These are then passed through a tube oven at 961^oC, the melting point of silver. Here, the agglomerates were converted to spherical nanoparticles by sintering and coalescence.

This polydisperse flow of nanoparticles was subjected to size selection using a Differential Mobility Analyzer (DMA). In the DMA, sheath air flow was used to drive the polydisperse flow of nanoparticles to be size selected based on their electrical mobility. By applying a particular DMA voltage, the electrical mobility and hence the size of the nanoparticle was selected. The ratio between the sheath air flow and polydisperse aerosol flow was adjusted to maintain a laminar flow. Thus nanoparticles of a particular size was selected for deposition. To determine the amount of silver nanoparticles for deposition, a condensation particle counter (CPC) was employed in setup design. This allowed for the counting of the nanoparticles of the intended size in P/ccm. For the deposition of nanoparticles, an electrostatic precipitator was used where the semiconductor substrate was mounted and deposition of nanoparticles occured because of the electric potential applied to the substrate. The no.of silver nanoparticles deposited were

approximately 7 to 8*10^9. The process conditions followed are detailed in table 3.1 as below

Parameter	Value
Spark frequency	2000 Hz
Carrier gas N_2 flowrate	4 LPM
Flow through DMA	2 LPM
Capacitor Voltage	1000 V
Oven Temperature	961 ^oC
Q_{sh}	9.01 LPM
Capacitor Voltage	1000 V

Table 3.1: Process conditions used in the generation of silver nanoparticles

3.3. Preparation of titanium dioxide by Atomic Layer Deposition[4]

Titanium dioxide semiconductor was prepared using the method of Atomic Layer Deposition(ALD). ALD was chosen based on its ability to develop coating of high quality with precise growth control. It is also recognised for the advantage posed with less waste created per product formed[62]. ALD is a self limiting growth technique where a precursor and co-reactant are involved in the reaction[63]. An ALD cycle typically consists of stages in the sequence of precursor-purge-co-reactant-purge. In this case, $TiCl_4$ was used as precursor and plasma as oxidiser/second reactant. A plasma enhanced ALD setup consisting of FlexAL ALD reactor (Flexible ALD in full form) (Oxford Instruments) was used with a remote inductively coupled plasma (ICP) source. Plasma allows ALD process to be caried at low temperature and remote source ensures low plasma damage. N_2 was used as purge gas to remove excess/ unreacted precursor and reaction byproducts in the cycle. A recipe in the software interface was followed to drive the experiment as per the process conditions. Titanium dioxide of 100 nm thickness was prepared for study. Table 3.2 gives the process conditions used in ALD.

Parameter	Value
Pressure	10^{-7} mbar
Temperature	100^oC
Sequence	700ms-4s-7s-6s
Duration of 1 cycle	17.7 s
No.of cycles	1000

Table 3.2: Process conditions used in ALD for preparation of titanium dioxide

To study the influence of change of refractive index of the surrounding, titania coating on silver nanoparticles was performed in a similar way but with the no. of ALD cycles reduced to 50.

A schematic illustration of the prepared photoanode $BiVO_4$ with silver-titanium dioxide functionalization is given in figure 3.3

3.4. Absorption via UV-Vis Spectroscopy

To determine the optical performance of the prepared semiconductor samples, the light absorption was measured using PerkinElmer-Lambda 900 UV-Vis spectrometer. Over a wave-

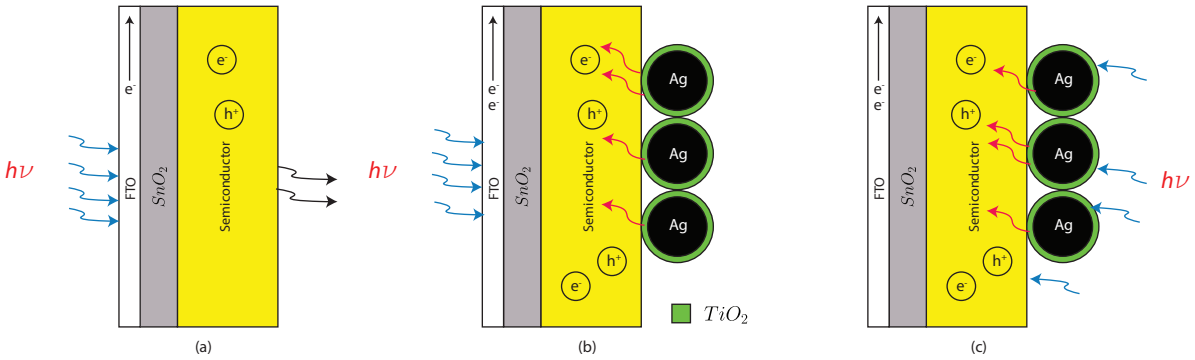

Figure 3.3: Schematic illustration of photoanode a)bare $BiVO_4$ b)$BiVO_4$ with Ag-TiO_2 for back illumination c)$BiVO_4$ with Ag-TiO_2 for front illumination. Blue arrows indicate incident photons, red arrows indicate scattered photons, black arrows indicate transmitted photons

length range of 350nm to 600nm of the solar spectrum, the optical spectra was analyzed. Using an integrating sphere where the sample was held in a holder, the absorption % of the sample was measured. Measurements were carried at room temperature for both front and back illumination of samples.

3.5. Photoelectrochemical cell

A three-electrode configuration was employed to build the photoelectrochemical cell. The cell was formed with the sample i.e., semiconductor as photoanode, Pt as counter electrode and Ag/AgCl (XR300,saturated KCl + AgCl solution (KS120), Radiometer Analytical) as reference electrode. Samples were placed in the cell exposed to illumination over an area of 0.283 cm^2. 0.1M potassium phosphate buffer solution with a pH of 7.2 was used as the electrolyte. The buffer solution was prepared by dissolving KH_2PO_4(99%, Sigma Aldrich) and K_2HPO_4(98%, Sigma Aldrich) in demineralized water. To study the Incident Photon to Current Efficiency (IPCE), a setup consisting of the following was used: 200 W quartz tungsten-halogen lamp, a multi-channelled potentiostat (Parstat MC,Princeton Applied Research), shutter device controller. The parameters used in the measurement are given in table 3.3 as follows To get the

Parameter	Value
Current auto limit	10 μA
Shutter time	10 s
Potential	1.23 V vs RHE
Start wavelength	600 nm
End wavelength	350 nm
Scan rate	18 nm/min

Table 3.3: Process conditions used in ALD of Titania on silver nanoparticles

j-V curve, Newport Sol3A Class AAA solar simulator(type 94023A-SR3) with simulated AM1.5 Solar illumination was used. Cyclic voltammetry scan with a scan rate of 0.1 V/s was performed on the samples. 5 ml of H_2O_2 was added to the electrolyte to perform as a hole scavenger, the implications of which are discussed in Chapter 4. All measurements were performed at room temperature.

4

Results and Discussion

The chapter deals with the results and discussion of the conducted experiments. Results pertaining to characterisation of nanoparticles, optical and photoelectrochemical experiments are discussed. For the study, silver nanoparticles of 3 different sizes, 43.5 nm, 72.4 nm and 78.5 nm were synthesized.

4.1. Characterisation of silver nanoparticles

To determine the size distribution of the generated nanoparticles, characterisation was performed under Transmission Electron Microscopy (TEM). The nanoparticles were deposited on copper TEM grids and loaded into airtight sample holder for analysis.

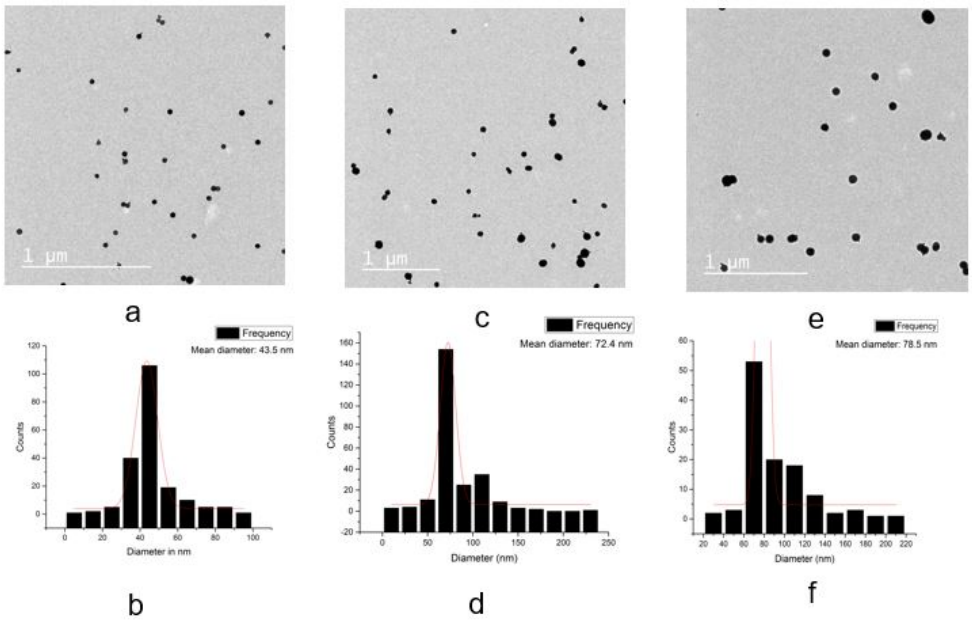

Figure 4.1: Size selected Ag nanoparticles produced by spark discharge and characterised under Transmission Electron Microscope a)43.5 nm Ag nanoparticles b)Particle size distribution of (a) c)72.4 nm Ag nanoparticles d)Particle size distribution of (c) e)78.5 nm Ag nanoparticles f)Particle size distribution of (e)

From figure 4.1, it is seen that single spherical nanoparticles are formed with exception to certain nanoparticles that have not been coalesced completely to form a sphere. The production of singlet nanoparticles by spark discharge is identified as in previous research conducted using

the technique [59][60]. A narrow size distribution is obtained which proves that nanoparticles of size fit for light scattering can be synthesized by the method of spark discharge. The images obtained under TEM were analyzed using ImageJ software.
It is to be noted that while performing the experiments to deposit silver nanoparticles on $BiVO_4$ substrate, the DMA was not grounded. This led to a slight variation in the particle size distribution obtained when compared to that obtained when DMA was grounded. However, since the change in variation was negligible, it was concluded that the change caused would not interfere in the study of light scattering.

4.2. Absorption and Scattering spectra

A theoretical modelling to obtain the absorption and scattering spectra was done to understand the size influence on the spectra. This is performed based on Mie's theory of scattering. From

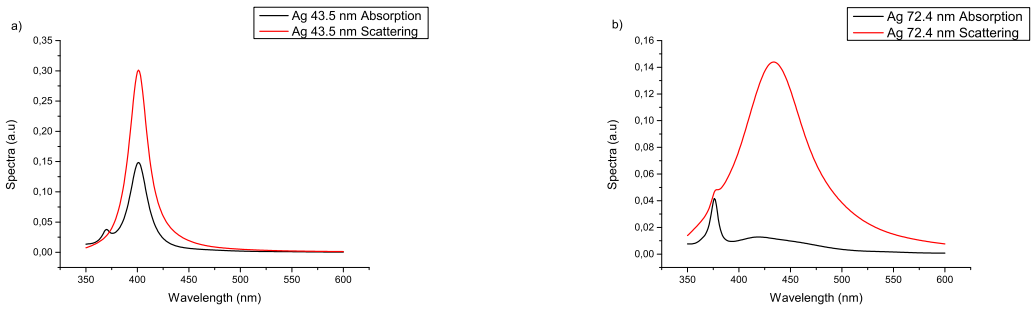

Figure 4.2: Absorption and scattering spectra for Ag nanoparticles simulated by Mie's theory in a surrounding of refractive index 1.33 a) 43.5 nm b) 72.4 nm

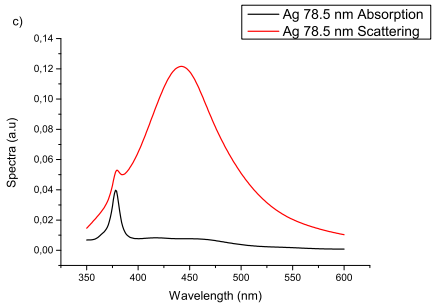

Figure 4.3: Absorption and scattering spectra for Ag nanoparticles simulated by Mie's theory in a surrounding of refractive index 1.33 c) 78.5 nm

figure 4.2 and 4.3, the influence of absorption and scattering spectra can be well identified. The ratio of the scattering and absorption spectra is seen to be increasing with increase in particle size. The surrounding refractive medium used in the simulation is that of water. This confirms that as the size of the nanoparticle increases, the scattering spectrum is more dominant than the absorption spectrum.

4.3. Light absorption

Absorption % is calculated as follows

$$A\% = 100 - T\% - R\% \tag{4.1}$$

To study the absorption of the semiconductor, the absorption% of FTO was first determined and subsequently subtracted from FTO-semiconductor absorption measurement. A compar-

ison of the A% of $BiVO_4$ and $BiVO_4$ coated with silver nanoparticles is shown in figure 4.4. Similarly, a comparison of TiO_2 and TiO_2 coated with silver nanoparticles is shown in figure 4.5. This optical performance will be explained in subsequent sections in the form of change in absorption.

Note: In all the figures corresponding to $BiVO_4$, the legend is represented as BVO in place of $BiVO_4$

The absorption change which is brought solely by silver nanoparticles is obtained by neglect-

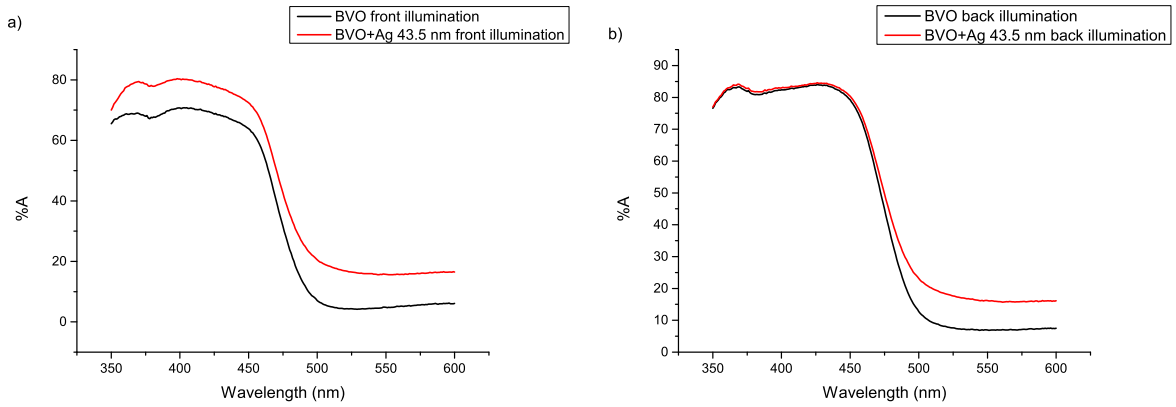

Figure 4.4: Comparison of absorption% for $BiVO_4$ and $BiVO_4$ deposited with 43.5 nm silver nanoparticle a) front illumination b) back illumination

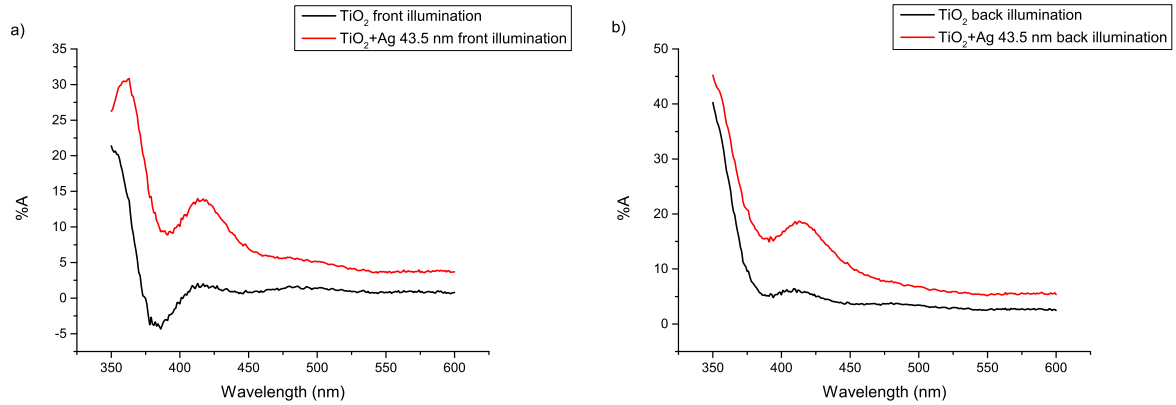

Figure 4.5: Comparison of absorption% for TiO_2 and TiO_2 deposited with 43.5 nm silver nanoparticle a) front illumination b) back illumination

ing that caused by FTO and semiconductor. Hence, it is calculated as

$$\Delta A\%_{Ag} = A\%_{FTO-SC-Ag} - A\%_{SC} - A\%_{FTO} \tag{4.2}$$

where SC stands for semiconductor $BiVO_4$ or TiO_2

4.4. Optical and Photoelectrochemical performance of $BiVO_4$ functionalized with silver nanoparticles

4.4.1. Front illumination

From figure 4.6, the increase in absorption for 43.5 nm silver nanoparticles is seen both in the 450-500 nm wavelength range and in the 350-375 nm range. This can be understood by

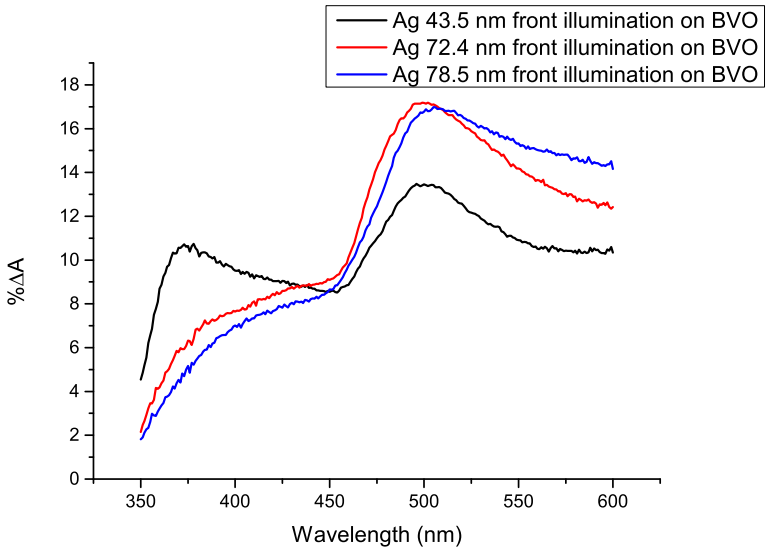

Figure 4.6: Change in absorption% caused by different sized nanoparticles deposited on $BiVO_4$ for front illumination

comparing the absorption % trend of $BiVO_4$ and $BiVO_4$-Ag samples. The increase in absorption within the bandgap of $BiVO_4$ where light absorption is high is attributed to the absorbing nature of the 43.5 nm silver nanoparticles, the smallest size of nanoparticle under investigation. Their scattering cross section is not well pronounced in this wavelength range. In the wavelength range of 450-500 nm which is the region of poor light absorption coefficient of $BiVO_4$, the enhanced increase in ΔA% is attributed to the surface plasmon resonance of silver. However, analysing the ΔA% of the 72.4 nm and 78.5 nm sized nanoparticle gives a clear picture about the effect of size of the nanoparticles on light absorption of $BiVO_4$. As the size of the nanoparticle increases, it is observed that the increase in absorption is pronounced effective in the region of poor light absorption. This denotes that the light scattering effect of the silver surface plasmon resonance is playing a role, noted in similar research as a broad enhancement within the bandgap of $BiVO_4$ [45].As the particle size increases,the scattering cross section also increases, meaning that bigger sized nanopartilces effectively scatter the incoming radiation into the underlying $BiVO_4$ layer. Also, a red shift in the spectrum is noticed with increase in particle size as per theory. Thus, the light which is incident on nanoparticles is first preferentially scattered by the nanoparticles into $BiVO_4$ which has a higher refractive index (2.45) than air, before it is available for absorption by $BiVO_4$. Key points to be noted from the front illumination experiment are the preferential scattering and anti-reflective nature of the deposited silver nanoparticles[39][47].

To be able to adequately prove that the optical effect of silver nanoparticles on the semiconductor will translate to the photoelectrochemcial effect, experiment to determine the IPCE% of the semiconductor-metal sample was performed. It is an essential photoelectrochemical measurement that gives the efficiency of current conversion from the incident photons. In order to entirely understand the effect of light scattering mechanism, it is necessary to ensure that the increase in photocurrent is caused only by an increase in $BiVO_4$ absorption (bulk effect) due to nanoparticle light scattering and not due to surface/catalytic effect.

To uncouple the catalytic effect from the bulk effect of silver nanoparticles, a hole scavenger is added to the electrolyte. H_2O_2 is used as hole scavenger where it functions by injecting the photogenerated holes at the semiconductor/ electrolyte interface. This ensures that surface transfer resistance and subsequently surface recombination are mitigated. The

rate constant of H_2O_2 oxidation is higher than that for water oxidation. Also, a relatively negative standard potential to release oxygen is an advantage for H_2O_2 when compared to 1.23 V for H_2O oxidation. Nearly 100% effciency of hole injection into the elctrolyte is facilitated by H_2O_2[15][64].

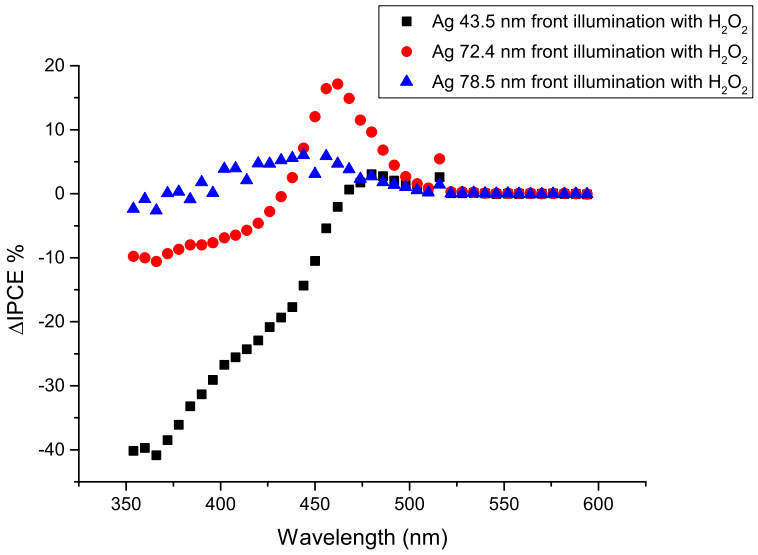

Figure 4.7: Change in IPCE% caused by different sized nanoparticles deposited on $BiVO_4$ for front illumination with hole scavenger H_2O_2

Figure 4.7 denotes the change in IPCE% with wavelength. This is obtained by taking into account the change brought by the silver nanoparticles. From the figure it is clear that for 43.5 nm sized nanoparticle, the change in IPCE% is negative in the range of wavelength of high light absorption by $BiVO_4$. However, the trend starts recovering toward the region of poor light absorption i.e 450-500nm. This is because, this sized nanoparticles act as screening particles on the $BiVO_4$ layer. This is verified from figure 4.6, where the increase in absorption of 43.5 nm nanoparticle corresponds with the decrease in current proving the screening of light. By screening the light to $BiVO_4$, the light is dominantly absorbed by these silver nanoparticles in front illumination. While comparing the change in IPCE% caused by the increased size of nanoparticles, it is seen that the 72.4 nm sized nanoparticle shows a clear increase in the wavelength range of interest and then a decrease. For the 78.5 nm sized nanoparticle case, the change is less, to the tune of 5% when compared to that of 17% caused by 72.4 nm sized nanoparticle. The reason is touted to be the interfacial area of contact per unit volume made by the silver nanoparticle with the $BiVO_4$ surface, which is higher for 72.4 nm particle than for 78.5 nm particle. This indicates that 72.4 nm particle has more preferential light scattering probability than 78.5 nm particle. The improvement in IPCE% in all the three cases is within the bandgap of $BiVO_4$ implying that the light scattering effect works only in the intended region of focus.

Figure 4.8 represents the APCE% for $BiVO_4$ and $BiVO_4$ with silver nanoparticle deposition for front illumination in the presence of H_2O_2. From this, it is clear that as IPCE% is corrected for the absorbed light efficiency, APCE% of scattering nanoparticle functionalized on $BiVO_4$ is similar to that of bare $BiVO_4$. In theory, the APCE% of $BiVO_4$ functionalized with scattering nanoparticles should be same as that of the bare $BiVO_4$, showing that the increase in current is because of increase in absorption[39]. In general, the measured APCE% of $BiVO_4$ with scattering size nanoparticle is similar or less than that of bare $BiVO_4$ as with increase in A%, increase in IPCE% is also noted, making the ratio close to that for bare $BiVO_4$. This

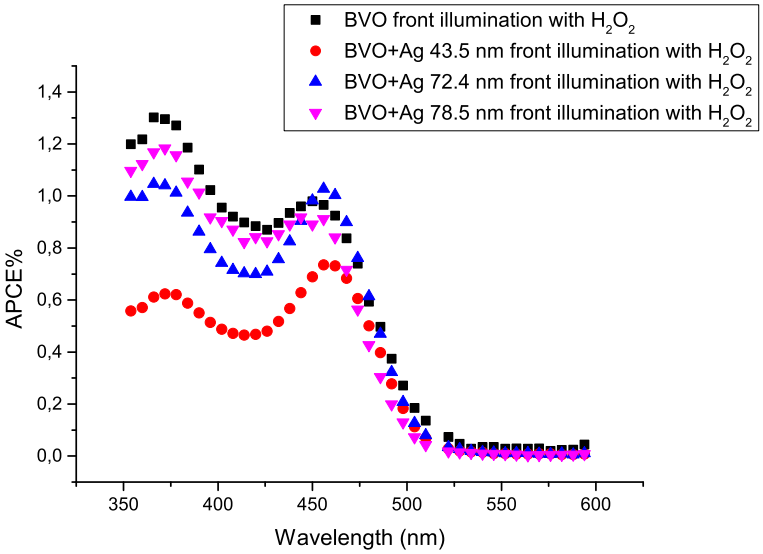

Figure 4.8: APCE% for $BiVO_4$ and $BiVO_4$ functionalized with silver nanoparticles for front illumination

observation is crucial to understand that as the size of the nanoparticle increases, the scattering efficiency increases thereby enhancing the light absorption of $BiVO_4$. With smaller sized nanoparticles barring light for semiconductor in front illumination, the rate of absorption of scattered photons remains low which translates into low photoelectrochemical performance of the semiconductor.This is a proof that the increase in IPCE% obtained in the presence of H_2O_2 is because of the absorption increase caused by preferential light scattering of nanoparticles. Current density obtained under AM1.5 solar illumination is represented in figure 4.9 against the applied potential V vs RHE. In plotting the j-V curve for $BiVO_4$, an average of four $BiVO_4$ samples was taken. This is to ensure that the deviation in the performance of the samples is taken into account. Anodic sweeps of the respective samples are plotted. The importance

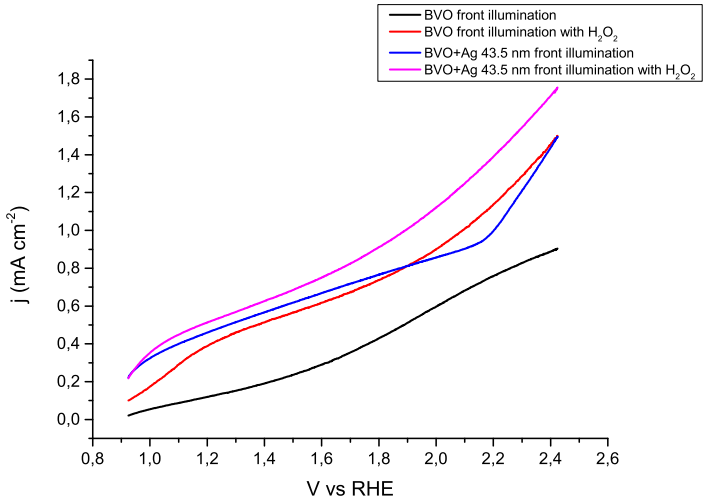

Figure 4.9: j-V sample curve for $BiVO_4$ and $BiVO_4$ coated with 43.5nm silver nanoparticles tested with and without hole scavenger H_2O_2.Cyclic voltammetry scan was performed at a scan rate of 0.1 V/s

of adding the hole scavenger is comprehended well , where the highest current density is obtained for $BiVO_4$-Ag with H_2O_2 implying that the photogenerated holes which reach the semiconductor/ electrolyte interface are successfully injected into the electrolyte to carryout the reaction. The change in current density at the water splitting potential i.e 1.23 V vs RHE is given in Appendix C, and not discussed here because of vagueness on the influence of size of nanoparticle.

4.4.2. Back illumination

Figure 4.10 gives the change in A% caused by the silver nanoparticles for back illumination. Here, the light is received by the semiconductor first and only the transmitted light reaches the nanoparticles. Marginal increase is clearly seen in the wavelength range of 450 – 500 nm. The steady increase seen in this region explicitly shows that silver nanoparticles preferentially back scatter the unabsorbed light into $BiVO_4$ improving the optical path length [39]. Below the optical bandgap edge of $BiVO_4$, light is completely available for silver nanoparticle unlike the transmitted light that was available after $BiVO_4$ absorption within the bandgap of semiconductor. The near flat profile of $\Delta A\%$ in the region where $BiVO_4$ strongly absorbs light shows that silver nanoparticles do not contribute to the light absorption in that region for back illumination

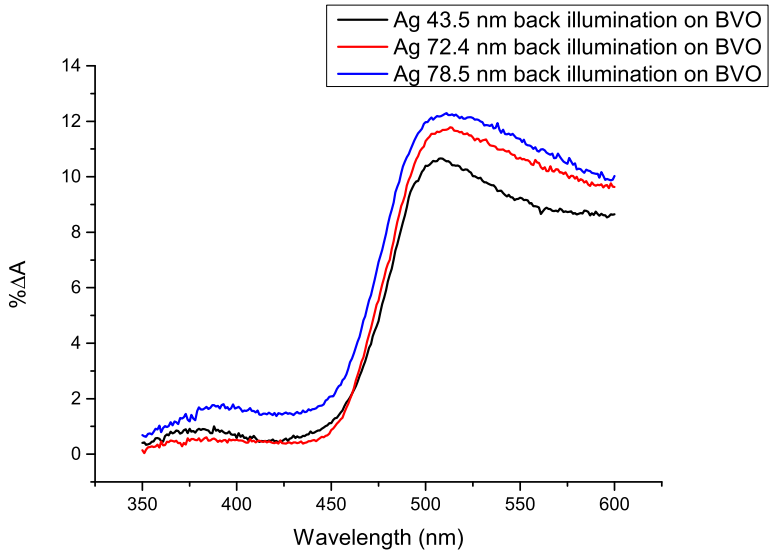

Figure 4.10: Change in absorption% caused by different sized nanoparticles for back illumination

It is to be noted that the power calibration corresponding to light intensity was not performed to compute the IPCE% as the cell design did not suit the setup to measure for back illumination. Figure 4.11 denotes the change in current measured under illumination against the wavelength. In this figure, it is seen that there is an increasing change in current for sizes 43.5 nm and 72.4 nm. But the least change in current for 78.5 nm which is puzzling because the change caused in light absorption differs from this point of view. Owing to the small interfacial area of contact per unit volume of the bigger nanoparticle with the semiconductor surface, it can be reasoned that the scattering into the semiconductor is not as effective as the other sized scattering nanoparticles. It can also be argued on the basis that the $BiVO_4$ samples used for the silver deposition was not uniform, which may be the reason for the drop in change in current in this case.
Current density noted for back illumination is presented in 4.12 wherein the magnitude is

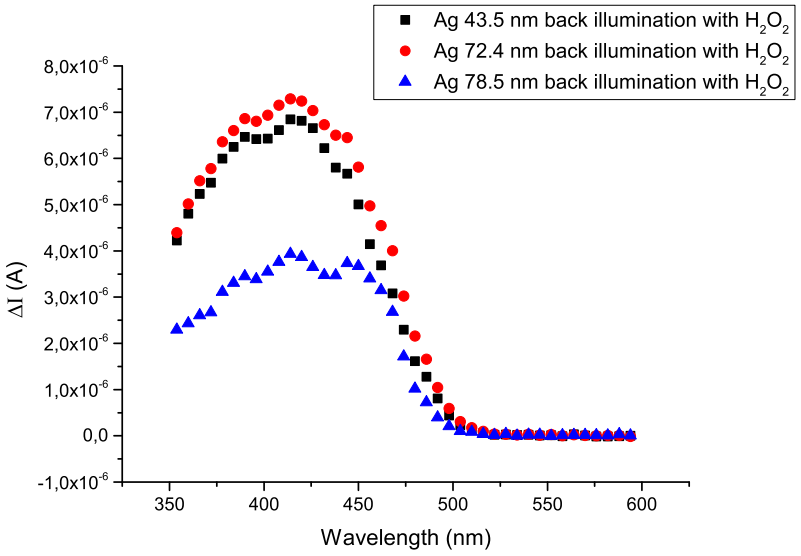

Figure 4.11: Change in current caused by different sized nanoparticles for back illumination with hole scavenger H_2O_2

higher than that obtained for front illumination. It is discussed on the same basis of increase in absorption for back illumination, where the $BiVO_4$ receives the entire spectrum of light first and the unabsorbed light is inturn scattered by the silver nanoparticles into its layer. The convex nature of the j-V curve shows that surface recombinations are mitigated by hole scavenger[65]. The change in current density obtained at water splitting potential of 1.23 V

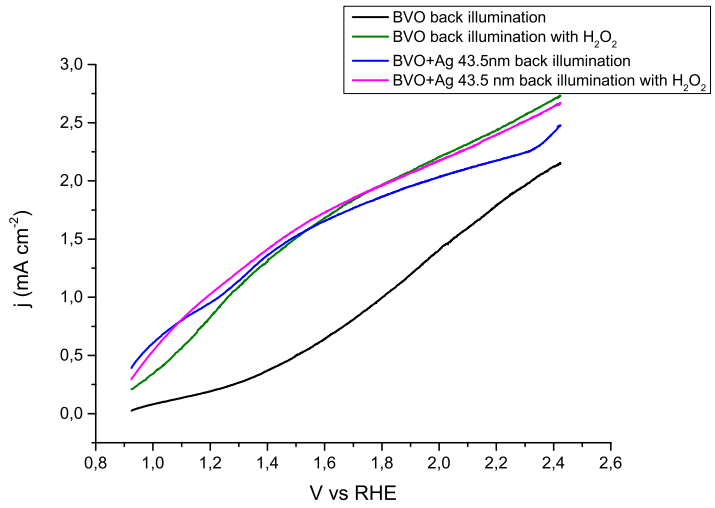

Figure 4.12: j-V sample curve for $BiVO_4$ and $BiVO_4$ coated with 43.5nm silver nanoparticles tested with and without hole scavenger H_2O_2. Cyclic voltammetry scan was performed at a scan rate of 0.1 V/s

vs RHE is given in Appendix C, for the reason that it gives no information about the influence of size of nanoparticle. It is hereby expressed that both for front and back illumination, the change in current density gives no fair insight about the effect of size of nanoparticle.

4.5. Comparison of light absorption of $BiVO_4$ and TiO_2 functionalized with silver nanoparticles

Figure 4.13 shows the change in absorption noted for the semiconductor samples $BiVO_4$ and TiO_2 after the deposition of silver nanoparticles. The bandgap edges corresponding to TiO_2 (3.2 eV) and $BiVO_4$ (2.4 eV) are denoted to understand the wavelength dependant absorption change. By depositing silver nanoparticle on both the semiconductors, it can be seen that the effect of size is different for the two semiconductors under study. It is seen that for TiO_2, the change in absorption% by silver is majorly focussed within its bandgap. The increase in absorption is because of absorption and/or scattering spectra of silver. The extension of light absorption beyond the bandgap of TiO_2 in the visible light region is due to the plasmonic nature of silver nanoparticles that are active in the SPR wavelength region. Also, with increase in the size of the nanoparticle, the increase in absorption change is reasoned as the size dependence on the extinction cross section of silver nanoparticle which is the sum of the absorption and scattering cross section. When comparing the contribution of silver nanoparticle to the increase in absorption in $BiVO_4$, it can be noticed that it is predominant below the optical absorption bandgap edge of $BiVO_4$. The steady increase noted in this wavelength range where $BiVO_4$ is characterised with low absorption coefficient (between 450-500nm) indicates that the role of silver surface plasmons is well pronounced.

By analyzing the trend of absorption increase for both the semiconductors, it is evident that if the increase would have been caused purely by light absorption of silver nanoparticles, it would be exactly at the same region for both the semiconductors. But it is seen that there is almost no visible optical response in the 450-500nm wavelength range for TiO_2 unlike in $BiVO_4$. From this, it is proved that the absorption increase noted in $BiVO_4$ is caused by nanoparticles that preferentially scatter the incident light into the semiconductor facilitating increased light absorption. The overlap of the plasmonic interaction of silver nanoparticle with the bandgap of $BiVO_4$ is understood to be the reason behind the absence of a separate silver SPR peak. This enhanced light absorption by $BiVO_4$ which is facilitated by the silver SPR drives absorption increase unlike the sole light absorption of silver, proving that the deposited nanoparticles are indeed scattering light.

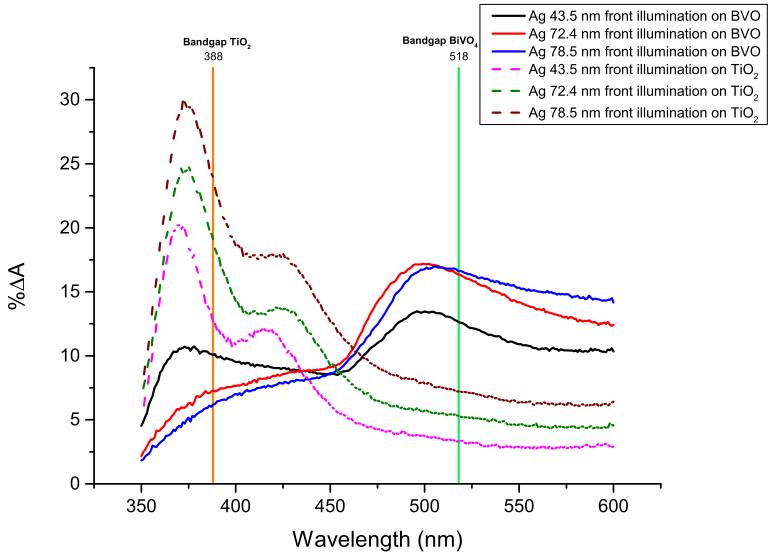

Figure 4.13: Change in absorption% caused by different sized nanoparticles deposited on TiO_2 and $BiVO_4$ for front illumination

Representing back illumination in figure 4.14 , the comparison of change in absorption for the semiconductors can also visualized with respect to the light scattering mechanism of silver SPR. The difference in absorption change trends is also in line with discussion presented for front illumination, where the increase in $BiVO_4$ light absorption is credited to the light scattering nature of silver nanoparticles.

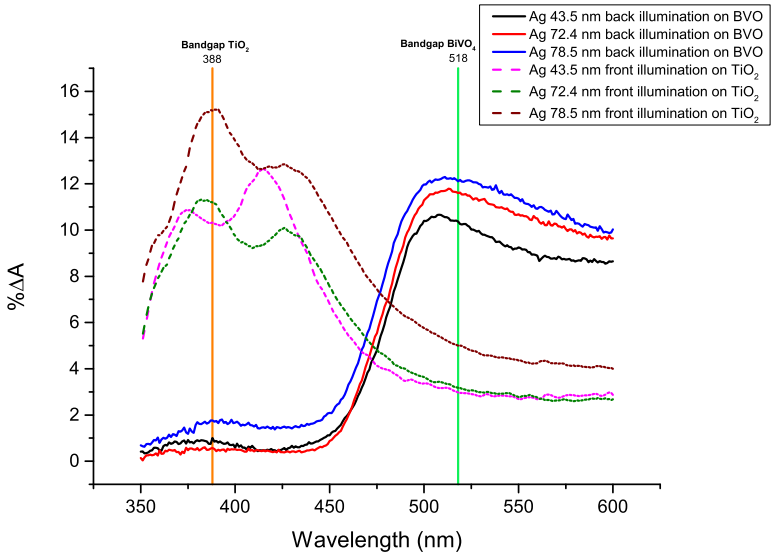

Figure 4.14: Change in absorption% caused by different sized nanoparticles deposited on TiO_2 and $BiVO_4$ for back illumination

4.6. Optical and Photoelectrochemical performance of TiO_2 deposited with silver nanoparticle

This section discusses the photoelectrochemical performance of TiO_2 functionalized with silver nanoparticle by comparing its optical performance. There is no separate discussion on the optical performance as it is already discussed in the previous section.

4.6.1. Front illumination

Figure 4.15 gives the change in IPCE% with wavelength for different sized nanoparticles deposited on TiO_2. Discussion can be followed that there is no increase in IPCE% effected by silver nanoparticles unlike that noticed in the case of $BiVO_4$. It is ideal to expect that even if the nanoparticles did not enhance the performance of TiO_2, it would not degrade the same, unlike the observation made here. The trend followed here shows that within the bandgap of TiO_2, the decrease is steep unlike the no change noticed outside the bandgap. This means that although the silver nanoparticles promoted increase in absorption of TiO_2 as shown in figure 4.16, this optical enhancement is not reflected in the photoelectrochemical performance. This can be argued on the basis that in front illumination where the silver nanoparticles receive the light first, they act as screening particles hindering oxygen evolution at the semiconductor electrolyte interface[47]. This suggests that the nanoparticles neither perform as catalyst to transport the photogenerated charge carriers to the electrolyte nor aid in the generation of new electron hole pairs. The size of the nanoparticle becomes relevant in the study where with increase in the size of the nanoparticle, there is a decrease in the interfacial contact area with the semiconductor. Thus as the size of the nanoparticle increases, the trend shifts upwards implying that smaller sized nanoparticle with high interfacial surface area with semiconductor

influences the surface effects of charge carrier transport greatly.

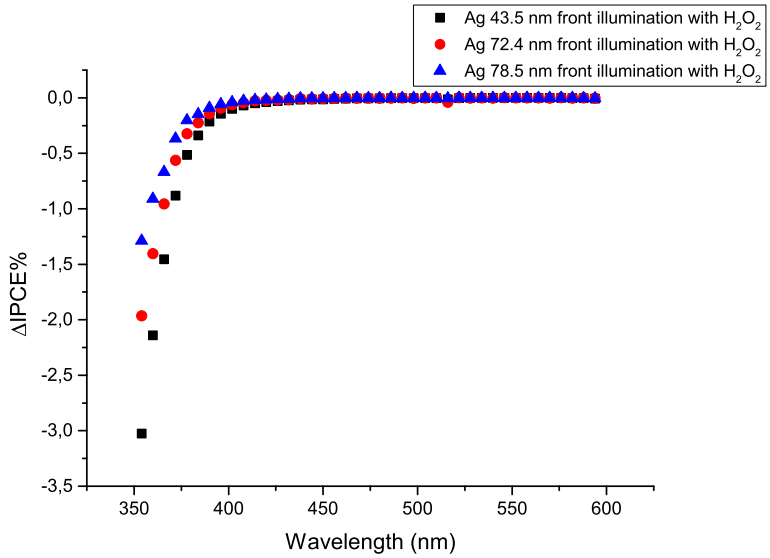

Figure 4.15: Change in IPCE% caused by different sized nanoparticles deposited on TiO_2 for front illumination with hole scavenger H_2O_2

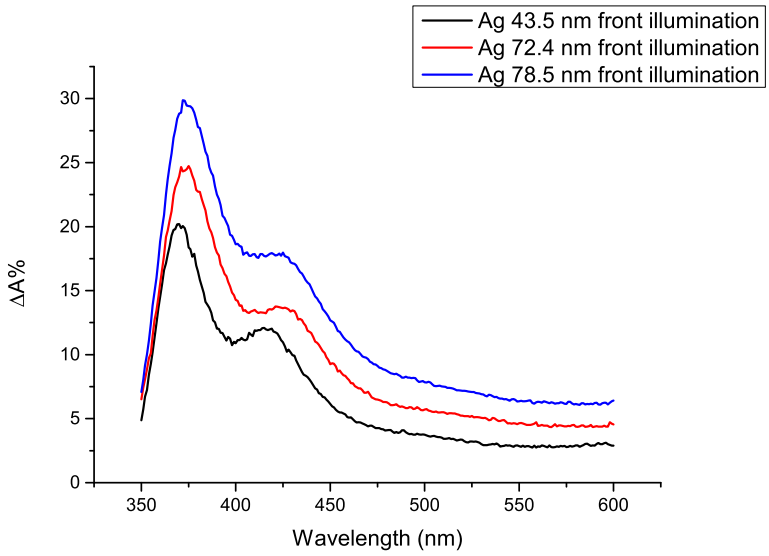

Figure 4.16: Change in absorption% caused by different sized nanoparticles deposited on TiO_2 for front illumination

Since there is no increase in IPCE in this case, there exists no requirement to perform APCE calculation.

4.6.2. Back illumination

Comparing the change in change in current performance for back illumination in figure 4.17, it can seen that there is a decreasing trend noticed likewise in front illumination. This was unexpected as the semiconductor receives the light first to generate charge carriers and allow the unabsorbed light for interaction with the nanoparticle. The absorption noted after nanoparticle

funtionalization in figure 4.18 shows marginal increase within the bandgap of TiO_2 and gradual decrease outside the bandgap. The correlation of the absorption increase with the size of the nanoparticle is not well defined but the indication of the increase in the optical band gap edge proves the function of silver plasmons. The decrease in the current obtained after deposition of nanoparticles indicate that the inherent nature of TiO_2 in generating electron hole pairs on irradiation is damaged. Although there is no strong reason as to why this happened, there is a speculation that the nanoparticles block the active sites of TiO_2, thereby directly affecting the photoelectrochemical performance.

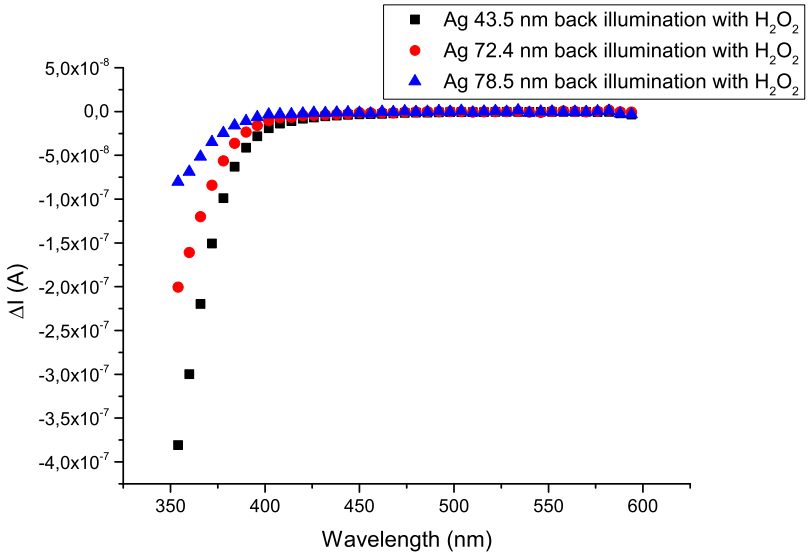

Figure 4.17: Change in current caused by different sized nanoparticles for back illumination with hole scavenger H_2O_2

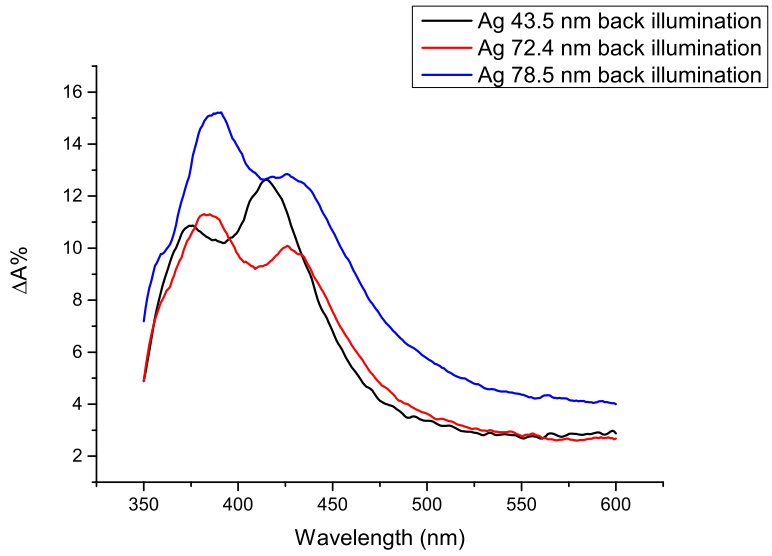

Figure 4.18: Change in absorption% caused by different sized nanoparticles for back illumination

4.7. Titania coating on silver nanoparticle

Coating of silver nanoparticle by Titania using Atomic Layer Deposition was done to obtain a homogeneous coating. Preliminary coating experiments were conducted to determine the influence of coating on the silver surface plasmon resonance. Characterisation of the coated sample under TEM is shown in figure 4.19

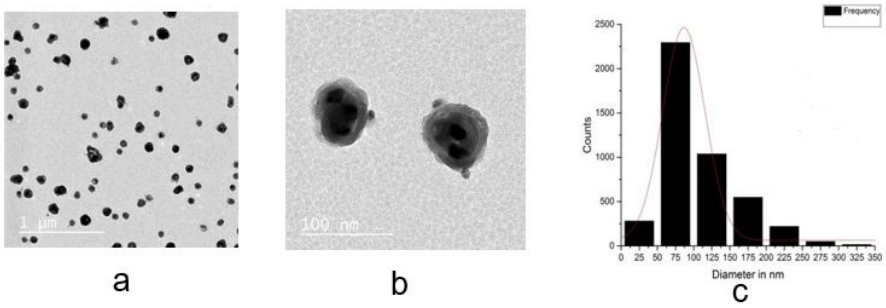

Figure 4.19: Size selected Ag nanoparticles produced by spark discharge and characterised under Transmission Electron Microscope a)43.5 nm Ag nanoparticles coated with TiO_2 b) TiO_2 coating over silver nanoparticle c)Particle size distribution of (a) with mean diameter of 86.5nm

From the particle size distribution obtained, it is clear that the particle size has grown double of the original silver nanoparticle. This could be because of particle migration or sintering during ALD. Analysing the sample under edX gave result where apart from the intended silver and titanium, chlorine also found its presence. The source of chlorine is precursor $TiCl_4$. This presence leads to a discussion whether the purging sequence of the ALD cycle was not effective to remove traces of the unreacted/ excess precursor in the ALD cycle.
The coating thickness is calculated to be 7.9 nm. This unexpected coating thickness hinders discussion on the optical and photoelectrochemcial effects of silver coated titania, where the results cannot be validated on the basis of the SPR effect of silver. As coating thickness depends on the no. of ALD cycles, it is inferred that by performing experiments with reduced no. of ALD cylces, a thin coating can be obtained. As reported in theory, coating thickness is a prime factor that affects the surface plasmon resonance of the metal. As the local electromagnetic field generated due to surface plasmon resonance would not be felt beyond the sensing distance, the effect of the coating becomes futile in influencing the SPR of silver[55][56].
Thus, conclusion is arrived where the desired coating thickness is crucial. Without the desired coating of around 2-3nm thickness, the effect of changing the dielectric medium around the silver nanoparticle finds no use in further analysis. The results obtained with respect to absorption are mentioned in Appendix A.

5

Conclusion and Recommendations

5.1. Conclusion

The possibility of using the surface plasmon resonance of noble metal nanoparticles to impart change in the optical properties of n-type semiconductor photoanodes $BiVO_4$ and TiO_2 was studied and presented. The nature of the surface plasmons to decay by the mechanism of light scattering in particular was studied by photoelectrochemical experiments alongside optical observation. $BiVO_4$ and TiO_2 were prepared by the method of spray pyrolysis and atomic layer deposition respectively. Characterisation of nanoparticles generated by the method of spark discharge proved that singlet spherical nanoparticles were synthesized for use as plasmonic structures.

The research yielded an understanding of light scattering mechanism and the effect of size of plasmonic metal nanoparticles on the influence of light absorption of the semiconductor materials under investigation. Optical absorption increase noted in the bandgap of both the semiconductors proved that spectral overlap of the surface plasmon resonance of silver nanoparticles was essential for this phenomenon. The change in absorption behaviour of same sized nanoparticle for different semiconductors proved that with increase in size of the nanoparticle, the increase in scattering spectra essentially determined the improvement in absorption in $BiVO_4$. This was verified after comparing the results of absorption obtained for TiO_2.

Use of IPCE and APCE measurements to determine the efficiency of the photoanode in water splitting verified that by depositing nanoparticle on the surface semiconductor, the behaviour of the semiconductor was modified. The performance trend was verified from the theory of surface plasmon resonance of silver which on irradiation gave rise to surface plasmons decaying by the mechanism of light scattering.

In front illumination, with the smallest size nanoparticle of 43.5 nm effecting a change by acting as screening particles, the IPCE of both $BiVO_4$ and TiO_2 showed that the efficiency decreased the most within the bandgap of the respective semiconductors. As the size of the nanoparticles increased, it was seen that the performance improved, yet not marginally increasing beyond that of bare semiconductors. It was also understood that the largest size nanoparticle of 78.5 nm imparted less IPCE owing to less interfacial area of contact per unit volume with the semiconductors.

In back illumination, the change in current after depositing nanoparticles on semiconductors gave different impact of nanoparticle size. For $BiVO_4$, the change in current was the least for the largest size nanoparticle owing to one of the following reasons of interfacial contact area per unit volume and sample non-uniformity. In the case of TiO_2, decrease in current was

noted after depositing nanoparticles. The reason was speculated as blockage of active sites of TiO_2 by silver nanoparticles.

The study of the effect of refractive index by using silver-titanium dioxide coating was not conclusive as desired thickness of TiO_2 coating was not obtained. Undesired change in the size of the plasmonic nanoparticles after coating hindered further study.

Thus, from this study it is understood that SPR can be effectively tuned by altering the size of light scattering nanoparticle and used in influencing the performance of spectral overlapping semiconductor.

5.2. Recommendations

It is imperative to understand this phenomenon of light scattering with further careful study on various parameters affecting surface plasmon resonance and photoelectrochemical performance. To obtain maximum efficiency by this method of light scattering nanoparticles influencing semiconductor performance, it is necessary to perform study with different parameters, such as size, shape and composition.

Based on the application of surface plasmon resonance of metal nanoparticles, the following recommendations are presented.

- Study of light scattering of silver nanoparticles of intermediate sizes ranging between 40 nm and 80 nm to understand optimum size of scattering nanoparticle providing maximum photoelectrochemical efficiency of the photoanode
- Comparison of performance of $BiVO_4$ and TiO_2 of similar thickness and study of plasmonic interaction with nanoparticles
- Optimization of experiments to coat TiO_2 of desired thickness on plasmonic nanoparticle to understand the effect of refractive index on the surface plasmon resonance
- Investigation of effect of light scattering of silver plasmonic nanoparticles exhibiting spectral overlap with favourable bandgap semiconductor for water oxidation like Fe_2O_3 ($\approx$ 2.1 eV)
- Use of different or alloyed plasmonic nanoparticles such as Au/Cu to understand light scattering on semiconductors with spectral overlap
- Study of the effect of size and composition of core shell plasmonic nanoparticles in the scattering regime with different shell materials
- Study of shape and composition of plasmonic nanoparticles capable of light scattering
- Study of stability of photoelectrochemical water splitting performance based on light scattering plasmons

Bibliography

[1] R. Van de Krol and M. Grätzel, *Photoelectrochemical hydrogen production*, Vol. 90 (Springer, 2012).

[2] K. L. Kelly, E. Coronado, L. L. Zhao, G. C. Schatz, *et al.*, *The optical properties of metal nanoparticles: the influence of size, shape, and dielectric environment,* Journal of Physical Chemistry B-Condensed Phase **107**, 668 (2003).

[3] F. F. Abdi and R. van de Krol, *Nature and light dependence of bulk recombination in co-pi-catalyzed bivo4 photoanodes,* The Journal of Physical Chemistry C **116**, 9398 (2012).

[4] M. N. Mirvakili, H. Van Bui, J. R. van Ommen, S. G. Hatzikiriakos, and P. Englezos, *Enhanced barrier performance of engineered paper by atomic layer deposited al2o3 thin films,* ACS applied materials & interfaces **8**, 13590 (2016).

[5] A. L. Linsebigler, G. Lu, J. T. Yates, *et al.*, *Photocatalysis on tio2 surfaces: principles, mechanisms, and selected results,* Chemical reviews **95**, 735 (1995).

[6] F. F. Abdi, L. Han, A. H. Smets, M. Zeman, B. Dam, and R. Van De Krol, *Efficient solar water splitting by enhanced charge separation in a bismuth vanadate-silicon tandem photoelectrode,* Nature communications **4** (2013).

[7] L. Yang, H. Zhou, T. Fan, and D. Zhang, *Semiconductor photocatalysts for water oxidation: current status and challenges,* Physical Chemistry Chemical Physics **16**, 6810 (2014).

[8] Y. Xu and M. A. Schoonen, *The absolute energy positions of conduction and valence bands of selected semiconducting minerals,* American Mineralogist **85**, 543 (2000).

[9] T. Hisatomi, J. Kubota, and K. Domen, *Recent advances in semiconductors for photocatalytic and photoelectrochemical water splitting,* Chemical Society Reviews **43**, 7520 (2014).

[10] B. J. Trześniewski and W. A. Smith, *Photocharged bivo 4 photoanodes for improved solar water splitting,* Journal of Materials Chemistry A **4**, 2919 (2016).

[11] A. Kudo, K. Ueda, H. Kato, and I. Mikami, *Photocatalytic o 2 evolution under visible light irradiation on bivo 4 in aqueous agno 3 solution,* Catalysis Letters **53**, 229 (1998).

[12] I. Cesar, A. Kay, J. A. Gonzalez Martinez, and M. Grätzel, *Translucent thin film fe2o3 photoanodes for efficient water splitting by sunlight: nanostructure-directing effect of si-doping,* Journal of the American Chemical Society **128**, 4582 (2006).

[13] P. E. de Jongh, D. Vanmaekelbergh, and J. J. Kelly, *Cu 2 o: a catalyst for the photochemical decomposition of water?* Chemical Communications , 1069 (1999).

[14] F. F. Abdi, T. J. Savenije, M. M. May, B. Dam, and R. van de Krol, *The origin of slow carrier transport in bivo4 thin film photoanodes: A time-resolved microwave conductivity study,* The Journal of Physical Chemistry Letters **4**, 2752 (2013).

[15] F. F. Abdi, N. Firet, and R. van de Krol, *Efficient bivo4 thin film photoanodes modified with cobalt phosphate catalyst and w-doping,* ChemCatChem **5**, 490 (2013).

[16] P. Bornoz, F. F. Abdi, S. D. Tilley, B. Dam, R. Van De Krol, M. Graetzel, and K. Sivula, *A bismuth vanadate–cuprous oxide tandem cell for overall solar water splitting,* The Journal of Physical Chemistry C **118**, 16959 (2014).

[17] S. J. Hong, S. Lee, J. S. Jang, and J. S. Lee, *Heterojunction bivo 4/wo 3 electrodes for enhanced photoactivity of water oxidation,* Energy & Environmental Science **4**, 1781 (2011).

[18] K. Zhang, X.-J. Shi, J. K. Kim, and J. H. Park, *Photoelectrochemical cells with tungsten trioxide/mo-doped bivo 4 bilayers,* Physical Chemistry Chemical Physics **14**, 11119 (2012).

[19] W. Luo, Z. Yang, Z. Li, J. Zhang, J. Liu, Z. Zhao, Z. Wang, S. Yan, T. Yu, and Z. Zou, *Solar hydrogen generation from seawater with a modified bivo4 photoanode,* Energy & Environmental Science **4**, 4046 (2011).

[20] T. W. Kim, Y. Ping, G. A. Galli, and K.-S. Choi, *Simultaneous enhancements in photon absorption and charge transport of bismuth vanadate photoanodes for solar water splitting,* Nature communications **6** (2015).

[21] T. W. Kim and K.-S. Choi, *Nanoporous bivo4 photoanodes with dual-layer oxygen evolution catalysts for solar water splitting,* Science **343**, 990 (2014).

[22] A. Fujishima, *Electrochemical photolysis of water at a semiconductor electrode,* nature **238**, 37 (1972).

[23] E. Lancelle-Beltran, P. Prené, C. Boscher, P. Belleville, P. Buvat, and C. Sanchez, *All-solid-state dye-sensitized nanoporous tio2 hybrid solar cells with high energy-conversion efficiency,* Advanced Materials **18**, 2579 (2006).

[24] S. Ito, S. M. Zakeeruddin, R. Humphry-Baker, P. Liska, R. Charvet, P. Comte, M. K. Nazeeruddin, P. Péchy, M. Takata, H. Miura, *et al.*, *High-efficiency organic-dye-sensitized solar cells controlled by nanocrystalline-tio2 electrode thickness,* Advanced Materials **18**, 1202 (2006).

[25] B. O'regan and M. Grfitzeli, *A low-cost, high-efficiency solar cell based on dye-sensitized,* nature **353**, 737 (1991).

[26] T. Morikawa, R. Asahi, T. Ohwaki, K. Aoki, and Y. Taga, *Band-gap narrowing of titanium dioxide by nitrogen doping,* Japanese Journal of Applied Physics **40**, L561 (2001).

[27] P. Szymanski and M. A. El-Sayed, *Some recent developments in photoelectrochemical water splitting using nanostructured tio2: a short review,* Theoretical Chemistry Accounts **131**, 1202 (2012).

[28] N. Serpone and A. Emeline, *Semiconductor photocatalysis□ past, present, and future outlook,* (2012).

[29] W. Choi, A. Termin, M. R. Hoffmann, *et al.*, *The role of metal ion dopants in quantum-sized tio2: correlation between photoreactivity and charge carrier recombination dynamics,* Journal of physical chemistry **98**, 13669 (1994).

[30] Y. Diamant, S. Chen, O. Melamed, and A. Zaban, *Core- shell nanoporous electrode for dye sensitized solar cells: the effect of the srtio3 shell on the electronic properties of the tio2 core,* The Journal of Physical Chemistry B **107**, 1977 (2003).

[31] A. K. Ghosh and H. P. Maruska, *Photoelectrolysis of water in sunlight with sensitized semiconductor electrodes,* Journal of the electrochemical society **124**, 1516 (1977).

[32] Y. Matsumoto, J. Kurimoto, Y. Amagasaki, and E. Sato, *Visible light response of polycrystalline tio2 electrodes,* Journal of The Electrochemical Society **127**, 2148 (1980).

[33] K. Liu, H. Fu, K. Shi, F. Xiao, L. Jing, and B. Xin, *Preparation of large-pore mesoporous nanocrystalline tio2 thin films with tailored pore diameters,* The Journal of Physical Chemistry B **109**, 18719 (2005).

[34] S. Linic, P. Christopher, and D. B. Ingram, *Plasmonic-metal nanostructures for efficient conversion of solar to chemical energy,* Nature materials **10**, 911 (2011).

[35] N. K. Allam, F. Alamgir, and M. A. El-Sayed, *Enhanced photoassisted water electrolysis using vertically oriented anodically fabricated ti- nb- zr- o mixed oxide nanotube arrays,* ACS nano **4**, 5819 (2010).

[36] D. Thrithamarassery Gangadharan, Z. Xu, Y. Liu, R. Izquierdo, and D. Ma, *Recent advancements in plasmon-enhanced promising third-generation solar cells,* Nanophotonics **6**, 153 (2017).

[37] C. F. Bohren and D. R. Huffman, *Absorption and scattering by a sphere,* Absorption and Scattering of Light by Small Particles , 82 (1983).

[38] W. R. Erwin, H. F. Zarick, E. M. Talbert, and R. Bardhan, *Light trapping in mesoporous solar cells with plasmonic nanostructures,* Energy & Environmental Science **9**, 1577 (2016).

[39] M. Valenti, E. Kontoleta, I. A. Digdaya, M. P. Jonsson, G. Biskos, A. Schmidt-Ott, and W. A. Smith, *The role of size and dimerization of decorating plasmonic silver nanoparticles on the photoelectrochemical solar water splitting performance of bivo4 photoanodes,* ChemNanoMat **2**, 739 (2016).

[40] C. Clavero, *Plasmon-induced hot-electron generation at nanoparticle/metal-oxide interfaces for photovoltaic and photocatalytic devices,* Nature Photonics **8**, 95 (2014).

[41] Y. Tian and T. Tatsuma, *Mechanisms and applications of plasmon-induced charge separation at tio2 films loaded with gold nanoparticles,* Journal of the American Chemical Society **127**, 7632 (2005).

[42] E. Kowalska, O. O. P. Mahaney, R. Abe, and B. Ohtani, *Visible-light-induced photocatalysis through surface plasmon excitation of gold on titania surfaces,* Physical Chemistry Chemical Physics **12**, 2344 (2010).

[43] S. K. Cushing, J. Li, F. Meng, T. R. Senty, S. Suri, M. Zhi, M. Li, A. D. Bristow, and N. Wu, *Photocatalytic activity enhanced by plasmonic resonant energy transfer from metal to semiconductor,* Journal of the American Chemical Society **134**, 15033 (2012).

[44] A. O. Govorov, G. W. Bryant, W. Zhang, T. Skeini, J. Lee, N. A. Kotov, J. M. Slocik, and R. R. Naik, *Exciton- plasmon interaction and hybrid excitons in semiconductor- metal nanoparticle assemblies,* Nano letters **6**, 984 (2006).

[45] F. F. Abdi, A. Dabirian, B. Dam, and R. van de Krol, *Plasmonic enhancement of the optical absorption and catalytic efficiency of bivo 4 photoanodes decorated with ag@ sio 2 core–shell nanoparticles,* Physical Chemistry Chemical Physics **16**, 15272 (2014).

[46] Z. Liu, W. Hou, P. Pavaskar, M. Aykol, and S. B. Cronin, *Plasmon resonant enhancement of photocatalytic water splitting under visible illumination,* Nano letters **11**, 1111 (2011).

[47] D. B. Ingram and S. Linic, *Water splitting on composite plasmonic-metal/semiconductor photoelectrodes: evidence for selective plasmon-induced formation of charge carriers near the semiconductor surface,* Journal of the American Chemical Society **133**, 5202 (2011).

[48] A. Bansal, J. S. Sekhon, and S. Verma, *Scattering efficiency and lspr tunability of bimetallic ag, au, and cu nanoparticles,* Plasmonics **9**, 143 (2014).

[49] K. Catchpole and A. Polman, *Design principles for particle plasmon enhanced solar cells,* Applied Physics Letters **93**, 191113 (2008).

[50] T. R. Jensen, M. L. Duval, K. L. Kelly, A. A. Lazarides, G. C. Schatz, and R. P. Van Duyne, *Nanosphere lithography: effect of the external dielectric medium on the surface plasmon resonance spectrum of a periodic array of silver nanoparticles,* The Journal of Physical Chemistry B **103**, 9846 (1999).

[51] J. J. Mock, D. R. Smith, and S. Schultz, *Local refractive index dependence of plasmon resonance spectra from individual nanoparticles,* Nano letters **3**, 485 (2003).

[52] M. Duval Malinsky, K. L. Kelly, G. C. Schatz, and R. P. Van Duyne, *Nanosphere lithography: effect of substrate on the localized surface plasmon resonance spectrum of silver nanoparticles,* The Journal of Physical Chemistry B **105**, 2343 (2001).

[53] E. Ringe, J. M. McMahon, K. Sohn, C. Cobley, Y. Xia, J. Huang, G. C. Schatz, L. D. Marks, and R. P. Van Duyne, *Unraveling the effects of size, composition, and substrate on the localized surface plasmon resonance frequencies of gold and silver nanocubes: a systematic single-particle approach,* The Journal of Physical Chemistry C **114**, 12511 (2010).

[54] G. Xu, M. Tazawa, P. Jin, S. Nakao, and K. Yoshimura, *Wavelength tuning of surface plasmon resonance using dielectric layers on silver island films,* Applied Physics Letters **82**, 3811 (2003).

[55] S. Angkaew and P. Limsuwan, *Preparation of silver-titanium dioxide core-shell (ag@ tio2) nanoparticles: Effect of ti-ag mole ratio,* Procedia Engineering **32**, 649 (2012).

[56] S. D. Standridge, G. C. Schatz, and J. T. Hupp, *Toward plasmonic solar cells: protection of silver nanoparticles via atomic layer deposition of tio2,* Langmuir **25**, 2596 (2009).

[57] L. Filipovic, *Topography simulation of novel processing techniques* (na, 2012).

[58] V. A. Vons, L. C. de Smet, D. Munao, A. Evirgen, E. M. Kelder, and A. Schmidt-Ott, *Silicon nanoparticles produced by spark discharge,* Journal of Nanoparticle Research **13**, 4867 (2011).

[59] J. Feng, G. Biskos, and A. Schmidt-Ott, *Toward industrial scale synthesis of ultrapure singlet nanoparticles with controllable sizes in a continuous gas-phase process.* Scientific reports **5**, 15788 (2014).

[60] S. Schwyn, E. Garwin, and A. Schmidt-Ott, *Aerosol generation by spark discharge,* Journal of Aerosol Science **19**, 639 (1988).

[61] G. Biskos, V. Vons, C. U. Yurteri, and A. Schmidt-Ott, *Generation and sizing of particles for aerosol-based nanotechnology,* KONA Powder and Particle Journal **26**, 13 (2008).

[62] A. Goulas and J. R. van Ommen, *Scalable production of nanostructured particles using atomic layer deposition [dagger],* Kona **31**, 234 (2014).

[63] M. Leskelä and M. Ritala, *Atomic layer deposition chemistry: recent developments and future challenges,* Angewandte Chemie International Edition **42**, 5548 (2003).

[64] H. Dotan, K. Sivula, M. Grätzel, A. Rothschild, and S. C. Warren, *Probing the photoelectrochemical properties of hematite (α-fe_2o_3) electrodes using hydrogen peroxide as a hole scavenger,* Energy & Environmental Science **4**, 958 (2011).

[65] J. Reichman, *The current-voltage characteristics of semiconductor-electrolyte junction photovoltaic cells,* Applied Physics Letters **36**, 574 (1980).

List of Symbols and Abbreviations

α	Particle Polarizibility	m^3
ϵ	dielectric constant	
η	Efficiency	
λ	wavelength	m
σ_{abs}	Absorption cross section	m^2
σ_{sca}	Scattering cross section	m^2
a	radius of the particle	m
A	Absorbance	
ALD	Atomic Layer Deposition	
AM	Air Mass	
APCE	Absorbed photon to current efficiency	
c	speed of light	m/s
C	Area	m^2
CB	Conduction band	
CE	Counter Electrode	
e	electron charge	J
eV	electron-volt	
E^o	Standard Reduction Potential	V
G	Gibbs free energy	J
h	Planck's constant	J/s
IPCE	Incident photon to current efficiency	
j	current density	mA cm^{-2}
k	wavenumber	m^{-1}
L_i	Geometric shape factor	
LPM	Litre per minute	
m	particle relative to the medium	
NHE	Normal Hydrogen Electrode	
P	Power	W
P/ccm	Particles per cubic centimeter	
Q_{ex}	excess flow	Litre per minute
Q_{sh}	sheath air flow	Litre per minute
R	Reflectance	
R_{H_2}	Rate of hydrogen production	moles/s
RHE	Reversible Hydrogen Electrode	
SPR	Surface Plasmon Resonance	
STH	Solar-to-Hydrogen	
UV	Ultraviolet	
T	Transmittance	
V	Voltage	
V_p	Volume of particle	m^3
VB	Valence band	

A

Appendix-Absorption of $BiVO_4$ with Ag-TiO_2 deposition

For the results concerning the absorption performance of TiO_2 samples in Chapter 4, this Appendix is used. The change in absorption % is listed in the following figures

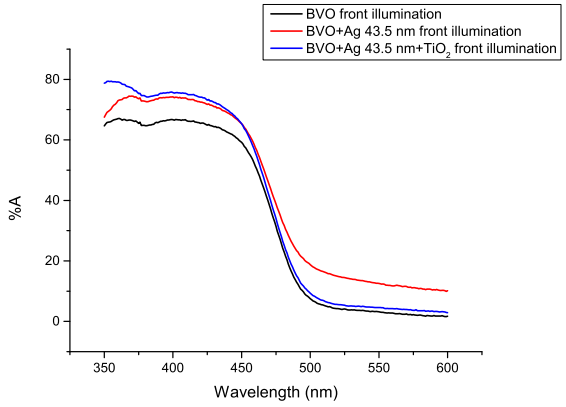

Figure A.1: Comparison of Absorption % for $BiVO_4$, $BiVO_4$ with 43.5 nm Ag and $BiVO_4$ with 43.5 nm Ag coated TiO_2 for front illumination

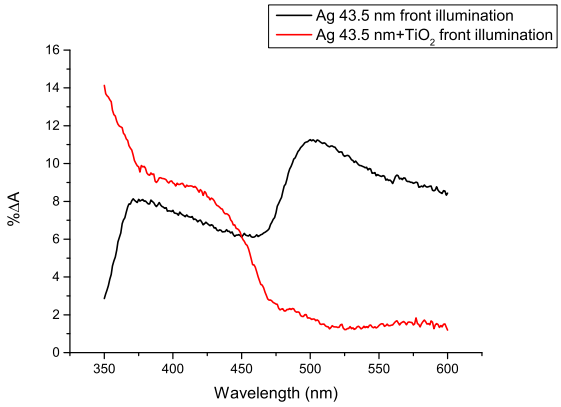

Figure A.2: Change in Absorption% for Ag 43.5 nm and Ag 43.5 nm coated with TiO_2 for front illumination

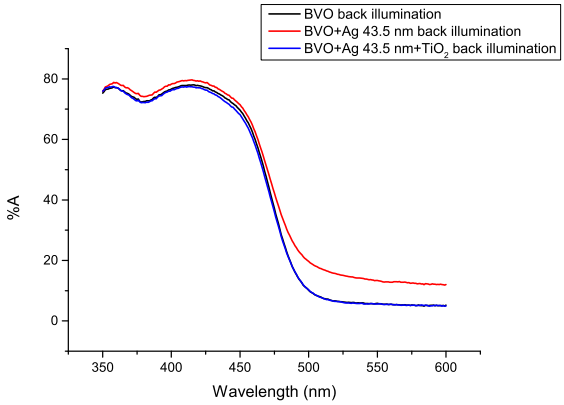

Figure A.3: Comparison of Absorption % for $BiVO_4$, $BiVO_4$ with 43.5 nm Ag and $BiVO_4$ with 43.5 nm Ag coated TiO_2 for back illumination

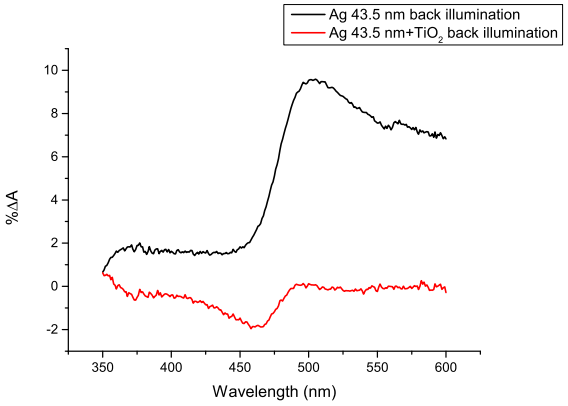

Figure A.4: Change in Absorption% for Ag 43.5 nm and Ag 43.5 nm coated with TiO_2 for back illumination

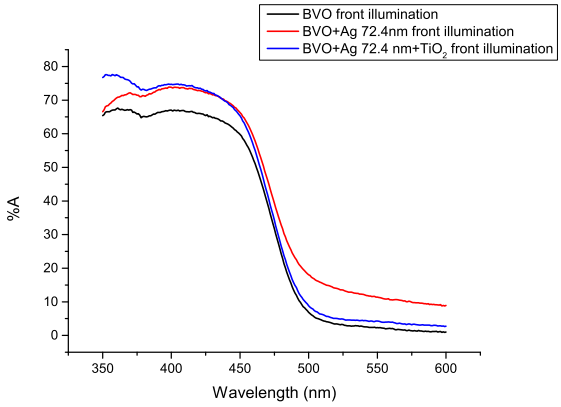

Figure A.5: Comparison of Absorption % for $BiVO_4$, $BiVO_4$ with 72.4 nm Ag and $BiVO_4$ with 72.4 nm Ag coated TiO_2 for front illumination

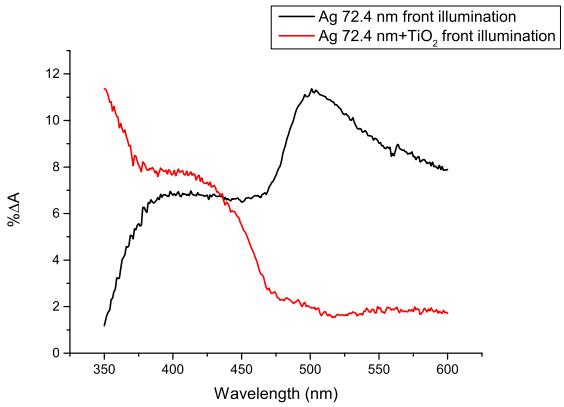

Figure A.6: Change in Absorption% for Ag 72.4 nm and Ag 72.4 nm coated with TiO_2 for front illumination

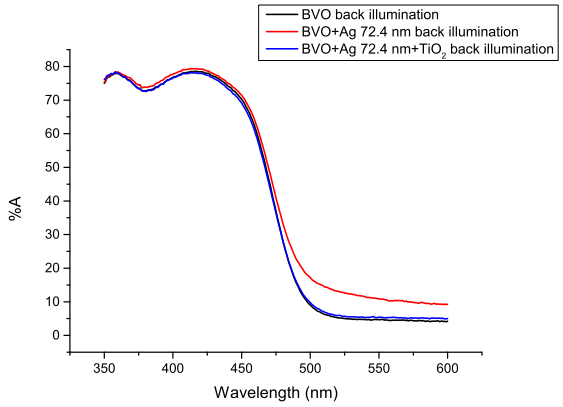

Figure A.7: Comparison of Absorption % for $BiVO_4$, $BiVO_4$ with 72.4 nm Ag and $BiVO_4$ with 72.4 nm Ag coated TiO_2 for back illumination

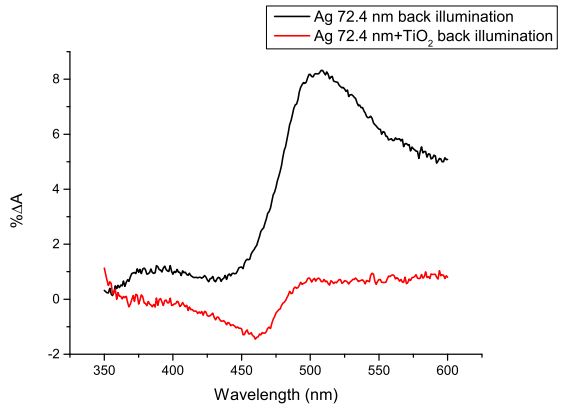

Figure A.8: Change in Absorption% for Ag 72.4 nm and Ag 72.4 nm coated with TiO_2 for back illumination

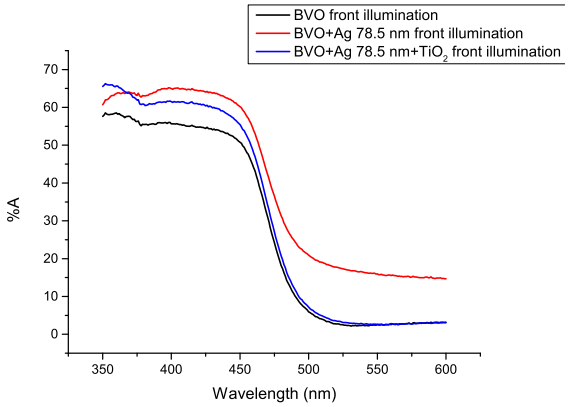

Figure A.9: Comparison of Absorption % for $BiVO_4$, $BiVO_4$ with 78.5 nm Ag and $BiVO_4$ with 78.5 nm Ag coated TiO_2 for front illumination

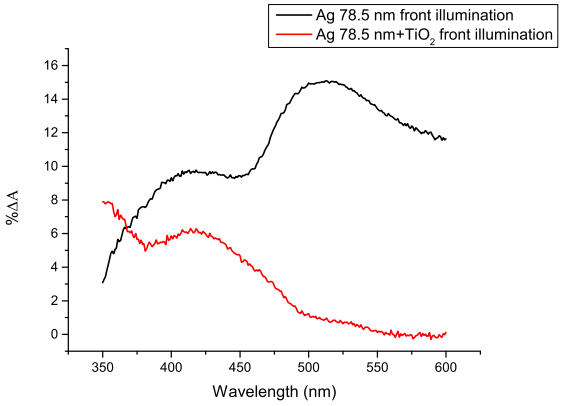

Figure A.10: Change in Absorption% for Ag 78.5 nm and Ag 78.5 nm coated with TiO_2 for front illumination

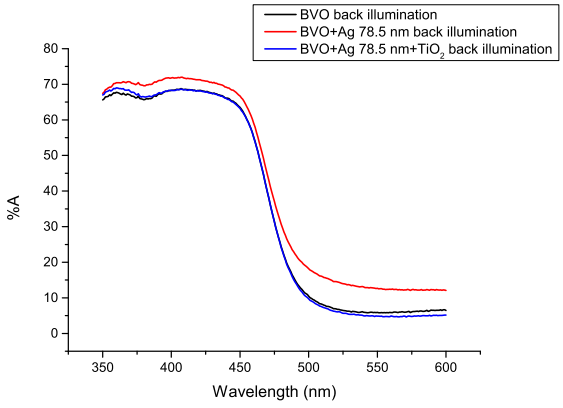

Figure A.11: Comparison of Absorption % for $BiVO_4$, $BiVO_4$ with 78.5 nm Ag and $BiVO_4$ with 78.5 nm Ag coated TiO_2 for back illumination

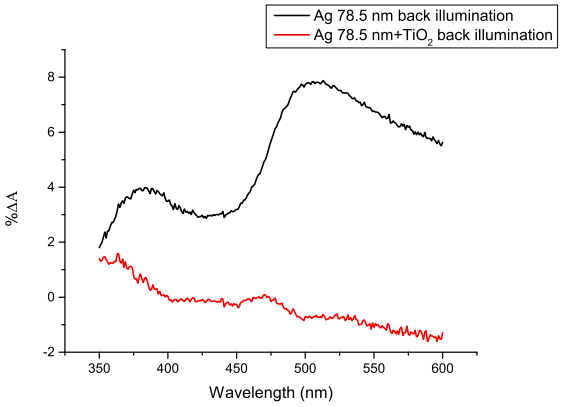

Figure A.12: Change in Absorption% for Ag 78.5 nm and Ag 78.5 nm coated with TiO_2 for back illumination

B

Appendix-Nanoparticle deposition

The nanoparticle deposition on $BiVO_4$ and TiO_2 was performed based on the parameters as shown in the table

Parameter	Ag 43.5 nm		Ag 72.4 nm		Ag 78.5 nm	
	$BiVO_4$	TiO_2	$BiVO_4$	TiO_2	$BiVO_4$	TiO_2
Flow(LPM)	1.721	1.8	1.737	1.754	1.728	1.782
Average (10^5 P/ccm)	3.471	2.376	1.304	1.325	1.053	0.762
Deposition time(min)	13	18	34	34	44	62

Table B.1: Generation of silver nanoparticles by spark discharge

C

Change in current density

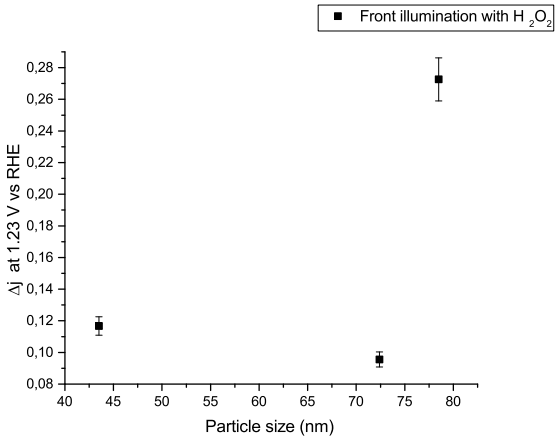

Figure C.1: Change in current density at 1.23 V vs RHE for $BiVO_4$ deposited with silver nanoparticle for front illumination

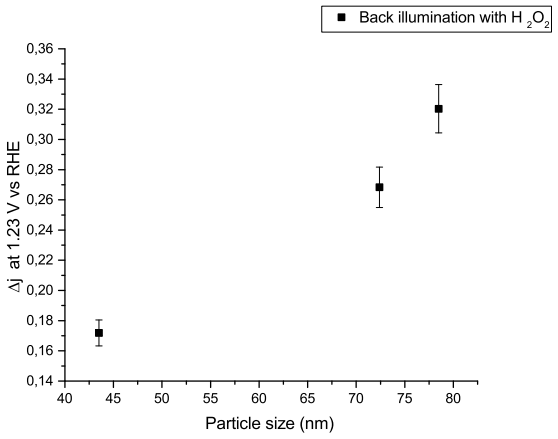

Figure C.2: Change in current density at 1.23 V vs RHE for $BiVO_4$ deposited with silver nanoparticle for back illumination